Knockdown of LINC00467 inhibits gastric cancer progression by modulating the sequestration of miR-141-3p

HUI JU[1], YI FENG[2], XIAOJING MU[3], WEITAI HE[4], GUIFANG HE[5], BEN TIAN[6], DUO CAI[5], CHANGCHANG LIU[5], YU SONG[5], HAO CHEN[7,8] and SHIHAI LIU[5]

[1]Department of Gastroenterology, The Affiliated Hospital of Qingdao University, Qingdao, Shandong 266500, P.R. China; [2]Department of Rehabilitation, The Affiliated Hospital of Qingdao University, Qingdao, Shandong 266500, P.R. China; [3]Department of Healthcare, The Affiliated Hospital of Qingdao University, Qingdao, Shandong 266500, P.R. China; [4]The Key Laboratory of Medicinal Resources and Natural Pharmaceutical Chemistry, The Ministry of Education, College of Life Sciences, Shaanxi Normal University, Xian, Shaanxi 710000, P.R. China; [5]Medical Animal Lab, Medical Research Center, The Affiliated Hospital of Qingdao University, Qingdao, Shandong 266500, P.R. China; [6]Department of Neurosurgery Intensive Medicine, The First Affiliated Hospital of Baotou Medical College, Baotou, Inner Mongolia Autonomous Region 014060, P.R. China; [7]Key Laboratory of Biomedical Information Engineering of Ministry of Education, Biomedical Informatics and Genomics Center, School of Life Science and Technology, Xi'an Jiaotong University, Xi'an, Shaanxi 710049, P.R. China; [8]Department of Technology Project, Research Institute of Xi'an Jiaotong University, Zhejiang 311215, P.R. China

Received January 11, 2025; Accepted May 9, 2025

DOI: 10.3892/ol.2025.15205

Abstract. Gastric cancer (GC) is one of the most common malignancies globally, with notable morbidity and mortality rates. Despite advances in surgical techniques and adjuvant therapies, recurrence and metastasis remain major challenges, highlighting the need for novel biomarkers and therapeutic targets. Long non-coding RNAs (lncRNAs) have emerged as key regulators in various types of cancer, including GC, which can influence tumor progression through diverse mechanisms. LINC00467, in particular, has been implicated in non-small cell lung cancer, hepatocellular carcinoma and colorectal cancer, but the role of LINC00467 in GC remains poorly understood. The present study aimed to elucidate the role of LINC00467 in GC progression by investigating its expression patterns, functional impact on cellular behaviors and underlying molecular mechanisms. The expression levels of LINC00467 were evaluated in the GEPIA database of human gastric cancer samples, which demonstrated LINC00467 upregulation in 60 tumor tissue samples from patients with GC compared with that of paired para-cancerous control tissues. Functionally, LINC00467 promoted glycolysis in GC cells and enhanced their proliferative, migratory and invasive activities. From a mechanistic perspective, LINC00467 was able to bind to microRNA (miR)-141-3p in GC cells and a negative correlation between miR-141-3p and LINC00467 expression was observed in GC tissue samples. Inhibition of miR-141-3p partially reversed the effects of LINC00467 knockdown on GC cell malignancy and LINC00467 was further found to control the expression of the miR-141-3p target gene dihydropyriminidase-like 3 (DPYSL3) in GC cells. Furthermore, lactate accumulation from glycolysis activated the AKT signaling pathway to promote the transcriptional expression of LINC00467 in GC cells and led to persistent glycolysis and GC cell invasion. The present study findings suggested that LINC00467 potentially controls GC progression via regulation of the miR-141-3p/DPYSL3 pathway.

Correspondence to: Professor Shihai Liu, Medical Animal Lab, Medical Research Center, The Affiliated Hospital of Qingdao University, 1677 Wutaishan Road, Qingdao, Shandong 266500, P.R. China
E-mail: shliumed@qdu.edu.cn

Key words: LINC00467, gastric cancer progression, microRNA-141-3p, dihydropyriminidase-like 3

Introduction

Gastric cancer (GC) is one of the most prevalent cancer types globally, with an estimated 0.97 million diagnoses and 0.66 million associated deaths in 2022 alone (1), which ranks fifth in terms of cancer incidence and cancer-related mortality (1). While GC is primarily treated through surgery, chemotherapy and radiotherapy, disease recurrence and metastasis affect ~50% of all patients after surgery, which result in poor survival outcomes (2,3). Thus, the identification of novel prognostic or diagnostic targets is necessary to improve survival outcomes in patients with GC.

Long non-coding RNAs (lncRNAs) have been found to be involved in cancer wherein the expression levels of lncRNAs benefitted the diagnosis, screening, and prognostic evaluation of patients (4,5). A previous study reported that the lncRNA, motor neuron and pancreas homeobox 1-antisense RNA1, was upregulated in GC tissues and was associated with poor patient outcomes (6), while the lncRNA, small nucleolar RNA host

gene 11, was identified as a potential diagnostic biomarker and therapeutic target for colon cancer (7). Furthermore, a subset of stroma-associated lncRNAs predicted disease recurrence and outcomes after adjuvant chemotherapy in patients with colon cancer (8).

Numerous studies have described the tumor-associated regulatory mechanisms mediated by lncRNAs and competitive endogenous RNAs (ceRNAs) (9-11). For example, GC metastasis-associated lncRNA serves as a ceRNA via sponging of micro RNA (miR)-124 and miR-34a in GC, while lncRNA hepatocyte nuclear factor 1 alpha antisense RNA 1 has been found to exert GC progression by regulating the expression of miR-30b-3p through the PI3K/AKT signaling pathway (10,12). In addition, lncRNAs can regulate gene expression by controlling the expression of miRNAs. For example, downregulation of lncRNA-activated by transforming growth factor TGF-β inhibits the epithelial-mesenchymal transition in breast cancer cells by promoting microRNA (miR)-141-3p expression (13). Furthermore, patterns of ceRNA regulation of LINC00467 have been described in various types of cancer, including non-small cell lung cancer (14), hepatocellular carcinoma (HCC) (15) and colorectal cancer (16). Given the direct relevance of lncRNAs to cancer-related outcomes, further research on associations with the diagnosis, treatment and prognostic evaluation of patients with GC is warranted to improve patient outcomes.

Several studies have reported that solid tumors, including GC, demonstrate notable metabolic changes associated with tumorigenesis, such as the utilization of glycolysis in addition to oxidative phosphorylation, even in the presence of abundant oxygen. This metabolic shift, known as aerobic glycolysis or the Warburg effect, represents a pivotal hallmark of tumor biology, which serves a key role in carcinogenesis, tumor progression and the development of drug resistance (17,18). Aerobic glycolysis facilitates rapid ATP synthesis, which induce alterations in the tumor microenvironment, promote biosynthesis and activate cell signaling pathways (19,20). However, despite extensive research on the fundamental role of aerobic glycolysis in cancer, understanding of the specific implication in GC remains limited. Therefore, further studies on the mechanistic underpinnings of glycolysis are necessary to enhance understanding of the complex processes involved in GC.

The present study aimed to explore the expression patterns, functional importance and mechanistic roles of LINC00467 in the context of GC progression, with a particular focus on the interaction between this lncRNA and miR-141-3p.

Materials and methods

Patient samples. GC tumor and para-cancerous tissue samples were collected from 60 patients treated in the Department of Pathology, The Affiliated Hospital of Qingdao University (Qingdao, China) between 2013 and 2015. Both primary tumors and metastatic lymph nodes were used to prepare tissue microarrays from formalin-fixed paraffin-embedded tissues. Patient follow-up data were obtained from the hospital's medical records and through direct communication with patients. The histopathological diagnosis and grading were performed by two experienced pathologists, and clinicopathological characteristics were recorded. The clinicopathological characteristics included age, sex, tumor differentiation degree, Lauren type, T stage, N stage, M stage and TNM stage (21). A total of 60 pairs of GC tissues and para-cancerous tissue samples were collected from patients who underwent surgery at the Affiliated Hospital of Qingdao University (Qingdao, China), and the present study cohort included 45 male and 15 female patients, with a median age of 64.42 years (mean ± SD, 64.42±10.11 years; range, 46-84 years). Survival data, such as overall survival (OS) and disease-free survival (DFS) were also collected to perform survival analysis via the Kaplan-Meier method and values were compared using the log-rank test. The studies involving human participants were reviewed and approved by The Ethics Committee at the Affiliated Hospital of Qingdao University (approval no. AHQDGC2019022; Qingdao, China). The patients provided their written informed consent to participate in the present study.

Bioinformatics analyses. The expression profile of LINC00467 was examined using 45 pairs of GC tissues and their corresponding normal adjacent tissues sourced from the GSE63089 database. The GSE63089 dataset (22) can be accessed through the Gene Expression Omnibus (GEO) on the NCBI website. The specific URL is https://www.ncbi.nlm.nih.gov/geo/query/acc.cgi?acc=GSE63089. This dataset contains expression data from 45 paired gastric cancer tissues and gastric normal tissues, which were used in the present study to examine the expression profile of LINC00467. The Gene Expression Profiling Interactive Analysis (GEPIA) online database (http://gepia2.cancer-pku.cn/#index) includes RNA-seq data on 9,736 tumor and 8,587 control tissue samples derived from The Cancer Genome Atlas Program (TCGA) and Genotype-Tissue Expression (GTEx) databases, which provide tools to enable gene expression profiling as a function of disease type or stage and to conduct corresponding analyses (23). The GEPIA database was utilized to assess LINC00467 expression profiles in 33 cancer types including GC, with $P<0.05$ as the significance threshold. In the bioinformatics analysis section, the MERAV database (http://merav.wi.mit.edu/) was also utilized for exploration analysis to assess LINC00467 expression in gastric cancer tissues. LINC00467-targeted miRNAs were predicted using miTarget (https://www.mitarget.org/), TargetScan (https://www.targetscan.org/vert_80/) and StarBase (https://rnasysu.com/encori/).

Subcellular localization prediction of LINC00467. The subcellular localization of LINC00467 was predicted using two online software tools: Genecards (https://www.genecards.org/, version accessed: 2025, database updated regularly) is a comprehensive genomic database providing gene annotation and functional prediction, including subcellular localization insights. RNALocate (http://www.rnalocate.org/, version 2.0, updated in 2023) is a specialized database for RNA subcellular localization, integrating experimental data and computational predictions. These tools were used to inform the design of subsequent FISH and nuclear/cytoplasmic fractionation experiments.

Cell culture and transient transfection. The AGS, HGC27 and MKN45 GC cell lines and the control GES-1 human cell line were from bnbio and were grown in DMEM (Gibco; Thermo

Fisher Scientific, Inc.) containing 10% FBS (Invitrogen; Thermo Fisher Scientific, Inc.) at 37˚C in a humidified 5% CO_2 incubator. Lipofectamine® 3000 (Invitrogen; Thermo Fisher Scientific, Inc.) was used for transient transfection of cells with siRNAs specific for LINC00467 (si-LINC00467), miR-141-3p mimics or inhibitors, or corresponding controls (si-NC, miR-NC and miR-NC inhibitor) from Shanghai GenePharma Co., Ltd. Detailed information regarding transfection sequences is provided in Table SI. siRNAs and mimics/inhibitors were transfected at a final concentration of 50 nM, unless otherwise specified in experiments. Transient transfections were performed using Lipofectamine 3000 (Invitrogen; Thermo Fisher Scientific, Inc.) according to the manufacturer's protocol. Briefly, cells were transfected at 70-80% confluence in serum-free medium for 6 h at 37˚C, after which the medium was replaced with fresh complete medium. For proliferation assays (RTCA, EdU and colony formation), cells were harvested at 24-72 h post-transfection. For migration/invasion assays (Transwell and wound healing), cells were analyzed at 48 h post-transfection. For qPCR and western blotting, samples were collected at 48 h post-transfection to assess gene/protein expression. For luciferase reporter assays, luciferase activity was measured 48 h after co-transfection of reporter vectors and oligonucleotides. These parameters were optimized to ensure efficient transfection and minimal cytotoxicity, with all experiments performed in triplicate unless stated otherwise.

Quantitative PCR (qPCR). The methods employed for qPCR have been previously described (24). An RNAiso kit (catalog no. 9109; Takara Bio, Inc.) was used to extract total RNA based on the manufacturer's protocol, after which cDNA was prepared from 1 μg of RNA with a TaqMan miRNA Reverse Transcription Kit (catalog no. 4366596; Applied Biosystems; Thermo Fisher Scientific, Inc.) for miRNA quantification assays, after which a TaqMan miRNA kit (catalog no. 15187092; Applied Biosystems; Thermo Fisher Scientific, Inc.) was used for qPCR analyses, with U6 used as a normalization control. For mRNA expression analyses, 2 μg of total RNA was reverse-transcribed using a PrimeScript first-strand cDNA synthesis kit (catalog no. K1622; Applied Biosystems; Thermo Fisher Scientific, Inc.), after which SYBR® Premix Ex Taq™ II (catalog no. RR0820; Applied Biosystems; Thermo Fisher Scientific, Inc.) was used to conduct qPCR, based on the manufacturer's protocol. The primers used are provided in Table SI. For the miRNA quantification assays, initial denaturation was performed at 95˚C for 10 min, followed by 40 cycles of denaturation at 95˚C for 15 sec and annealing/extension at 60˚C for 1 min. For the mRNA expression analyses, initial denaturation was performed at 95˚C for 30 sec, followed by 40 cycles of denaturation at 95˚C for 5 sec and annealing/extension at 60˚C for 30 sec. All analyses were conducted using a LightCycler 480 (Roche Diagnostics GmbH). GAPDH was used to normalize mRNA expression levels and the $2^{-\Delta\Delta Cq}$ method used to calculate relative gene expression (25).

Real-time cell analysis (RTCA) proliferation assay. An xCELLigence system E-Plate RTCA (Roche Diagnostics GmbH) was used to monitor proliferation (26) by assessing impedance values in each well and these results were used to calculate cell index (CI) values. Briefly, cells were plated at $1x10^4$ cells/well and grown for 24 h, after which they were treated with si-LINC00467, si-NC, miR-141-3p mimics, miR-141-3p inhibitors or corresponding control oligonucleotides using Lipofectamine 3000 and the CI was monitored for 15 h. CI values were used for normalization of the proliferation data.

Clonogenic assay. For HGC27 cells, colony formation assays were performed as follows. Human gastric HGC27 cells were seeded into 6-well plates at a density of 4,000 cells per well in DMEM (Gibco; Thermo Fisher Scientific, Inc.) supplemented with 10% FBS (Invitrogen; Thermo Fisher Scientific, Inc.). After 24 h of incubation at 37˚C in a humidified 5% CO_2 atmosphere to allow cell attachment, the medium was replaced with fresh complete medium. Cells were then cultured for 10 days under the same conditions (37˚C, 5% CO_2), with treatments including transfection of si-LINC00467, si-NC, miR-141-3p mimics, miR-141-3p inhibitors or corresponding controls as described in the experimental design. Following incubation, colonies were fixed with 70% ethanol at room temperature for 5 min to preserve cell morphology. Fixed colonies were stained with 0.05% crystal violet at room temperature for 10 min, allowing visualization of cell clusters. Colonies were defined as aggregates containing ≥50 cells. Images were captured using a brightfield microscope, and colonies were manually counted to quantify proliferation capacity, with colony diameters measured to assess growth efficiency. Data are presented as the mean ± SD from triplicate wells.

5-Ethynyl-2'-deoxyuridine (EdU) incorporation assay. Plates were not coated with any substrate prior to cell seeding. Experiments were performed using standard tissue culture-treated 24-well plates. Human gastric cancer AGS and HGC27 cell lines were used. siRNA oligonucleotides (si-LINC00467 and si-NC) and miRNA mimics/inhibitors (miR-141-3p mimics, inhibitors and miR-NC) were transfected at a 50 nM final concentration (Shanghai GenePharma Co., Ltd.) All images were captured at x100 magnification using a Nikon Eclipse Ti fluorescence microscope (Nikon Corporation). A 100-μm scale bar was included in each figure panel to indicate magnification. Images were acquired from 5 random fields per well using NIS-Elements software (Nikon Corporation). Values were averaged across triplicate wells for each condition. Cells were not serum-starved prior to or during the assay. Cells were maintained in DMEM supplemented with 10% FBS throughout the experiment to ensure optimal proliferation. An EdU kit (BeyoClick™ EdU Cell Proliferation Kit; Beyotime Institute of Biotechnology) was used to assess GC cell proliferative activity. Briefly, human gastric cancer AGS or HGC27 cells were added to 24-well plates ($2x10^4$/well) and were treated as appropriate for 72 h, after which EdU was added for 3 h at 37˚C. Cells were then fixed for 15 min with 4% paraformaldehyde at room temperature, permeabilized with 0.3% Triton X-100 for 15 min, combined for 30 min with click reaction mixture and stained for 10 min with Hoechst 33342. The cells were imaged using fluorescence microscopy and the number of proliferating cells was averaged to calculate the labeling index. Labeling Index was calculated as: Labeling Index=(total number of Hoechst-stained nuclei/number of EdU-positive cells) x100. Values were averaged across

triplicate wells for each condition. Statistical analysis was performed using GraphPad Prism 6 (Dotmatics).

Wound healing assay. Appropriately treated cells were added to 6-well plates and grown to confluence, at which time a sterile pipette tip was used to generate a scratch wound in the monolayer. Loose cells were washed away with PBS and fresh medium was then added. After 24 and 48 h post-wounding, the monolayer was imaged with a light microscope (ECLIPSE Ts2 microscope; Nikon Corporation).

Transwell assays. GC cell migration and invasion were assessed using Transwell assays. Briefly, complete DMEM was added to the lower chambers of wells in a 24-well plate, with GC cells ($2x10^4$ in 200 μl) added to the upper chamber of a Transwell insert. For invasion assays, Transwell inserts (8-μm pores) were precoated with Matrigel (BD Biosciences, San Jose, CA) diluted 1:8 with cold serum-free DMEM and incubated at 37˚C for 1 h to allow the Matrigel to solidify into a gel; for migration assays, inserts were uncoated. The plates were then incubated at 37˚C in a humidified 5% CO_2 incubator for 24 or 48 h to assess migration or invasion, after which cells on the upper surface were removed with a cotton swab and remaining cells were fixed with 4% paraformaldehyde prior to being stained for 15-20 min with 0.5% crystal violet (w/v) at room temperature for 20 min, rinsed with PBS, and imaged using a brightfield light microscope (Nikon Eclipse Ts2) at x100 magnification.

Luciferase reporter assay. GC cells were added to 24-well plates overnight. Cells were then co-transfected with pGL6-miR containing wild-type (WT) or mutated (Mut) sequences of the DPYSL3 3'-UTR or LINC00467 binding region, along with miR-141-3p mimics, miR-141-3p inhibitors, or corresponding miR-NC controls using Lipofectamine® 3000 Transfection Reagent (catalog no. L3000008; Invitrogen; Thermo Fisher Scientific, Inc.) according to the manufacturer's instructions. At 48 h post-transfection, luciferase activity was measured using the Dual-Luciferase Reporter Assay System (catalog no. E1910; Promega Corp.), with firefly luciferase activity normalized to *Renilla* luciferase activity to account for transfection efficiency. Data were expressed as the ratio of firefly to *Renilla* luciferase activity.

Fluorescence in situ hybridization (FISH). GC cells were first treated under non-denaturing conditions and were then hybridized with LINC00467 probes (Shanghai GenePharma Co., Ltd.). The procedures were performed in accordance with the manufacturer's instructions. DAPI (1:1,000) was then used to stain nuclei for 5 min, after which a confocal microscope (Leica Biosystems) was used to image the cells. ImageJ (National Institutes of Health) was used to analyze the images to assess the subcellular localization of LINC00467.

Western blotting. Protein samples were isolated from GC cell lines (AGS and HGC27) at 48 h after transfection. Cells were lysed in RIPA Lysis Buffer (catalog no. P0013B; Beyotime Institute of Biotechnology) containing 1X Protease Inhibitor Cocktail (catalog no. P2417; MilliporeSigma) on ice for 30 min, followed by centrifugation at 12,000 x g for 15 min at 4˚C. Supernatant protein concentrations were quantified using the BCA Protein Assay Kit (catalog no. 23225; Thermo Fisher Scientific, Inc.). Equal amounts of protein (30 μg/sample) were separated on 10% gels using SDS-PAGE and transferred to PVDF membranes (MilliporeSigma). Blots were blocked with 5% non-fat milk for 1 h in TBST at room temperature for 1 h, after which they were stained with anti-DPYSL3 (catalog no. ab126787; Abcam) and anti-GAPDH (catalog no. #2118; Cell Signaling Technology, Inc.). After washing, membranes were incubated with HRP-linked goat anti-mouse IgG (1:2,000; catalog no. 7076; Cell Signaling Technology, Inc.) or HRP-linked goat anti-rabbit IgG (1:2,000 dilution; catalog no. 7074; Cell Signaling Technology, Inc.) at room temperature for 1 h each. An enhanced chemiluminescence kit (catalog no. BB-3501; Cytiva) was used to detect protein bands, with Image Lab 2.0 (Bio-Rad Laboratories, Inc.) used for data analysis. GAPDH served as a loading control.

Biotinylated miRNA pulldown assay. Cells were transfected with biotinylated miR-141-3p mimics or miR-141-3p mutants using Lipofectamine® 3000 (Invitrogen; Thermo Fisher Scientific, Inc.). After 48 h, the cells were collected, washed with PBS and lysed on ice for 15 min. Following centrifugation, 100 μl aliquots of the lysates were reserved as input samples. The remaining samples were incubated with M-280 streptavidin-coupled Dynabeads™ (Invitrogen; Thermo Fisher Scientific, Inc.) at 4˚C for ~3.5 h. Subsequently, the bound RNA was eluted using wash buffer and TRIzol® (Beyotime Institute of Biotechnology) was used to purify the RNA for subsequent analysis. The biotinylated miR-141-3p mimics and mutants were synthesized by Guangzhou RiboBio Co., Ltd.

RNA immunoprecipitation assay. Cells were transfected with miR-141-3p mimics and the miR-141-3p mutant using Lipofectamine® 3000 (Invitrogen; Thermo Fisher Scientific, Inc.). After 48 h, argonaute 2 (AGO2) immunoprecipitation was performed using an RNA immunoprecipitation kit (catalog no. P0101; Guangzhou Geneseed Biotech. Co., Ltd.) according to the manufacturer's protocol. Antibodies against IgG (catalog no. ab172730; Abcam) and anti-AGO2 (catalog no. ab32381; Abcam) were obtained. Lysates (500 μg total protein) were incubated overnight at 4˚C with 30 μl Protein A/G magnetic beads pre-bound to either 5 μg anti-AGO2 antibody (catalog no. ab186733; Abcam) or 5 μg IgG control (catalog no. ab172730; Abcam). Beads were washed sequentially with Wash Buffers 1-3. Bound RNA-protein complexes were eluted by incubation. Input (10% of total lysate) served as the positive control. The input was utilized as the positive control and IgG served as the negative control. To confirm the efficiency of immunoprecipitation, Western blotting was conducted using the anti-AGO2 antibody and the harvested RNAs were subjected to qPCR for further analysis.

Glucose uptake, lactate production and ATP production assays. GC cells were seeded at $1x10^4$ cells per well in 96-well plates and analyzed using a colorimetric glucose uptake assay kit (catalog no. 36503; AAT Bioquest, Inc.) and a colorimetric L-lactate assay kit (catalog no. 13815; AAT Bioquest, Inc.) following the manufacturer's instructions. For the ATP assay, $3x10^5$ cells cultured in 6-well plates were lysed in 200 μl/well

lysis buffer on ice and the lysates were subsequently centrifuged at 4˚C. The ATP content in the supernatant was determined using an enhanced ATP assay kit (catalog no. S0027; Beyotime Institute of Biotechnology) according to the manufacturer's protocol. The content was normalized to the cell number. Each experiment was performed in quintuplicate.

Assays of extracellular acidification rate (ECAR) and oxygen consumption rate (OCR). The ECAR and cellular OCR were assessed using the Seahorse XFe 96 Extracellular Flux Analyzer (Seahorse Bioscience; Agilent Technologies, Inc.) according to the manufacturer's protocol. ECAR and OCR were determined using Seahorse XFe Glycolysis Stress Test Kit (cat no. 103020-100; Agilent Technologies) and Seahorse XF Cell Mito Stress Test Kit (cat no. 103015-100; Agilent Technologies), respectively. Briefly, $1x10^4$ cells per well were seeded into a Seahorse XFe 96 cell culture microplate (Seahorse Bioscience; Agilent Technologies, Inc.). After baseline measurements, for ECAR, glucose, the oxidative phosphorylation inhibitor oligomycin and the glycolytic inhibitor 2-deoxyglucose (2-DG) were sequentially injected into each well at indicated time points; and for OCR, oligomycin, the reversible inhibitor of oxidative phosphorylation p-trifluoromethoxy carbonyl cyanide phenylhydrazone (FCCP) and the mitochondrial complex I inhibitor rotenone plus the mitochondrial complex III inhibitor antimycin A (Rot/AA) were sequentially injected.

In the measurements of glycolysis, a stepwise injection protocol was employed to examine the metabolic behavior of cells. Glucose was administered, at a final concentration of 10 mM per well, to initiate the glycolytic process. Subsequently, oligomycin was introduced, with a final concentration of 2 μM per well, to inhibit ATP synthase and redirect energy production towards glycolysis. Finally, 2-DG was injected at a final concentration of 50 mM per well. Prior to these injections, cells were cultured in XF Glycolysis stress test assay medium devoid of glucose to maintain appropriate cellular conditions. During the first injection, glucose underwent catabolism via the glycolytic pathway, which resulted in the generation of pyruvate along with ATP, NADH, water and protons. The subsequent injection of oligomycin specifically hindered mitochondrial ATP synthesis, thereby promoting a shift in energy production towards glycolysis. This shift enabled assessment of the cellular maximum glycolytic capacity. By comparing the measurements of glycolysis with the glycolytic capacity, the extent of the glycolytic reserve can be determined.

The initial introduction of oligomycin (2 μM final concentration per well), an ATP synthase inhibitor, led to a reduction in oxygen consumption rate associated with mitochondrial respiration and ATP production. Subsequently, the administration of FCCP (1 μM final concentration per well), an uncoupling agent, caused the collapse of the proton gradient and mitochondrial membrane potential. This disruption allowed for unimpeded electron flow through the electron transport chain, which maximized oxygen utilization by complex IV and yielded peak respiration. The disparity between the basal respiration and the maximal respiration levels determined the spare respiratory capacity, which represented the respiratory capability available to meet increased energy demands. In the last injection stage, Rot/AA (0.5 μM final concentration per well), was introduced. This combination completely halted mitochondrial respiration and facilitated the calculation of non-mitochondrial respiration attributed to processes occurring outside the mitochondria. Data were analyzed by Seahorse XFe 96 Wave software (version 2.6.1; Agilent Technologies, Inc.). ECAR was presented in mpH/min and OCR was presented in pmols/min.

Xenograft model studies. HGC27 cells that had been transduced with sh-LINC00467 or sh-NC were subcutaneously implanted into the right flanks of 4-week-old male BALB/c nude mice (18-20 g body weight; Viltalriver Inc.), with each mouse receiving $5x10^6$ cells in 150 μl of FBS-free culture medium. A total of 12 mice (6 per experimental group) were used. Mice were housed in a climate-controlled facility (22±2˚C; 55±5% humidity; 12 h light/dark cycle) with free food and water access. Tumors were measured twice per week, with tumor volume being defined as tumor volume=(width x width x length)/2. Each experimental group included 6 mice. On day 22 post-implantation, mice were anesthetized using 1% sodium pentobarbital (50 mg/kg, Sigma-Adrich; Merck KGaA), a method widely accepted for rodent anesthesia (27). Following anesthesia, cervical dislocation was performed to ensure complete cessation of life. The largest volume measured was 808.195 mm^3 and the largest diameter measured was 11.93 mm. Subsequently, tumors were excised and weighed for further analysis. The Ethics Committee of the Affiliated Hospital of Qingdao University approved the present animal study (approval no. AHQU-MAL20190810; Qingdao, China).

Statistical analysis. SPSS (version 19.0; IBM Corp.) and GraphPad Prism 6 (version 6; Dotmatics) were used for all statistical analyses. Correlations between patient clinicopathological features (age, sex, differentiation grade, Lauren type, T stage, N stage, M stage and TNM stage) and LINC00467 expression were assessed via χ^2 tests, while other differences between groups (e.g., si-NC vs. si-LINC00467, miR-NC vs. miR-141-3p mimics/inhibitors), clinical stage groups (e.g., TNM stage I/II vs. III/IV), cell line groups (e.g., GC cells vs. GES-1) and *in vivo* groups (e.g., sh-NC vs. sh-LINC00467 mice) were compared using unpaired Student's t-test and one-way ANOVA followed by Tukey's post hoc test. Paired t-tests were used to compare gene expression between tumor and adjacent normal tissues from the same patients (LINC00467 expression in 60 GC tumor/paracancerous tissue pairs; miR-141-3p expression in the same 60 paired samples). For non-paired datasets (e.g., MERAV), unpaired t-tests were performed to assess group differences. Spearman's correlation analyses were used to evaluate the association between LINC00467 and miR-141-3p or DPYSL3 in tumors. $P<0.05$ was considered to indicate a statistically significant difference.

Results

LINC00467 is upregulated in human GC. In pursuit of identifying key lncRNAs implicated in the advancement of GC, a comprehensive analysis was conducted utilizing microarray data on gene expression encompassing 45 pairs of GC tissues and their corresponding normal adjacent tissues (GSE63089). Notably, LINC00467 exhibited upregulation (logFC=0.2982;

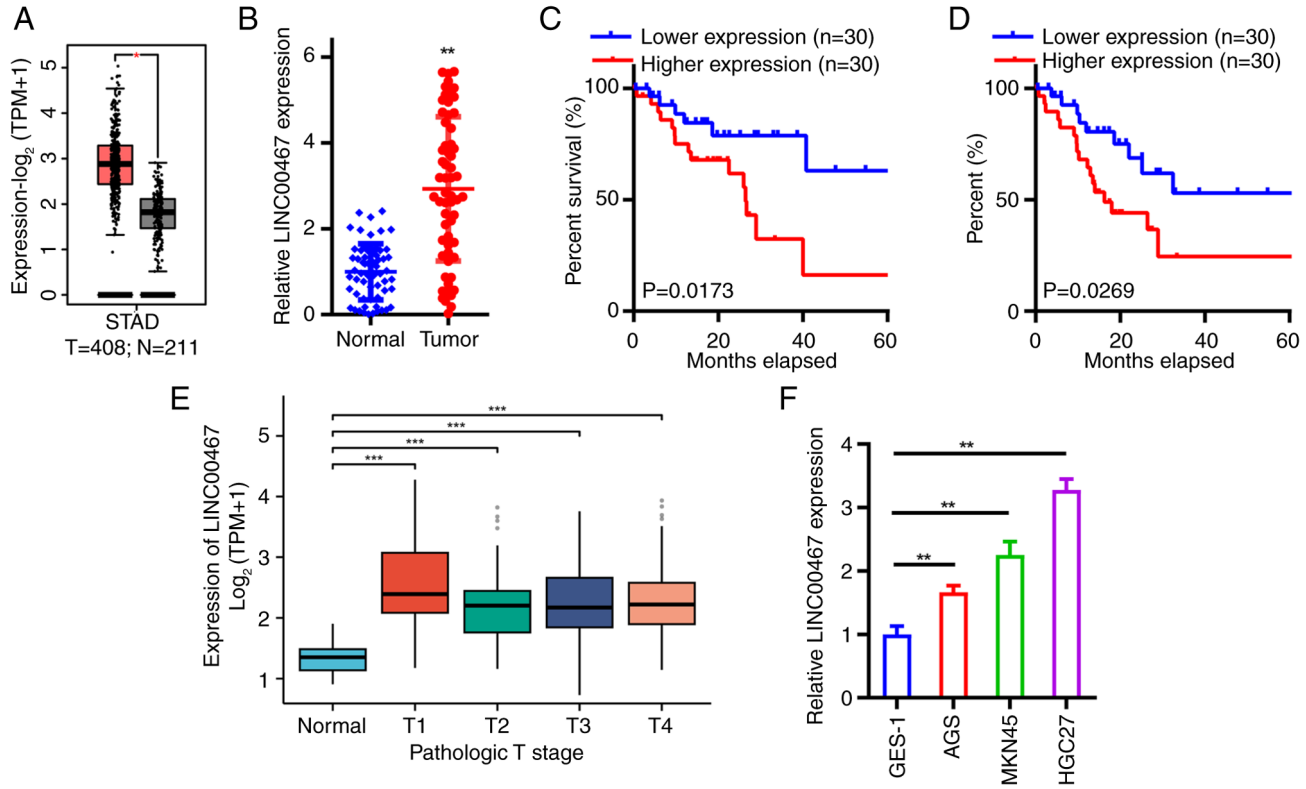

Figure 1. LINC00467 is upregulated in GC tissues and associates with GC progression. (A) LINC00467 levels in STAD (n=408) and normal tissue samples (n=211) in the GEPIA database. (B) Relative LINC00467 levels in 60 pairs of GC tumor tissue and para-cancerous samples. (C) Patient survival percentage (n=60) was assessed using Kaplan-Meier curves and log-rank tests. Lower LINC00467 expression (n=30) was represented in blue and higher LINC00467 expression (n=30) was represented in red. (D) Analysis of DFS in patients with GC based on relative LINC00467 expression levels. Lower expression (n=30) was represented in blue and higher expression (n=30) was represented in red. (E) Expression levels of LINC00467 across different T stages (T1-T4) and in normal tissues. (F) Relative LINC00467 expression levels were assessed in AGS, HGC27 and MKN45 human GC cells and in GES-1 control cells. *P<0.05; **P<0.01; ***P<0.001. GC, gastric cancer; STAD, stomach adenocarcinoma; GEPIA, Gene Expression Profiling Interactive Analysis; DFS, disease-free survival.

P=0.0025) within GC tissues (Fig. S1A-B). Subsequent exploration within the GEPIA and MERAV databases demonstrated an increased expression of this lncRNA within GC tumor tissues compared with that of normal tissue (Figs. 1A and S1C). Furthermore, expression pattern analyses of tumor and normal tissues sourced from the TCGA and GTEx databases demonstrated a consistent upregulation of LINC00467 in comparison to adjacent normal tissues across 16 cancer types: Breast invasive carcinoma, cervical and endocervical cancer types, colorectal adenocarcinoma, lymphoid neoplasm diffuse large B-cell lymphoma, esophageal carcinoma, glioblastoma multiforme, liver HCC, lung adenocarcinoma, ovarian serous cystadenocarcinoma, pancreatic adenocarcinoma, rectum adenocarcinoma, skin cutaneous melanoma, stomach adenocarcinoma, thymoma, uterine corpus endometrial carcinoma and uterine carcinosarcoma (Fig. S1D).

To elucidate the regulatory mechanisms governing the LINC00467 molecule in GC, a comprehensive examination of LINC00467 expression levels was conducted utilizing qPCR on a cohort of 60 freshly frozen GC tissues. This cohort consisted of 20 cases from clinical stages I and II, alongside 40 cases from clinical stages III and IV (as detailed in Table I). Subsequently, the association between LINC00467 and the clinicopathological characteristics of GC were explored. The analysis (Table I) demonstrated significant associations between LINC00467 expression and the N stage (P=0.015) as well as the TNM stage (P=0.028). Nevertheless, the expression pattern of LINC00467 was not significantly associated with age (P=0.791), sex (P=0.371), differentiation (P=0.184), Lauren type (P=0.688), T stage (P=0.278), or M stage (P=0.085).

Consistent with these results, qPCR results indicated significant upregulation of LINC00467 in 60 GC tumor tissues compared with para-cancerous normal samples (Fig. 1B; P<0.0001). Patients were then stratified into LINC00467-low (n=30) and -high (n=30) groups based on median LINC00467 expression. Survival analysis using Kaplan-Meier curves suggested that high LINC00467 expression in patients was associated with significantly shorter OS and DFS (P<0.05; Fig. 1C and D). The expression levels of LINC00467 were further analyzed across different T stages (T1-T4) and compared with normal tissues in the TCGA database. The results demonstrated a significant upregulation of LINC00467 in tumor tissues compared with normal tissues (P<0.001). However, no significant differences were observed between different T stages within the tumor group, which suggested that the LINC00467 is primarily upregulated in the presence of tumors rather than varying significantly across tumor stages (Fig. 1E). LINC00467 was similarly upregulated in three GC cell lines compared with that of control GES-1 gastric cells, with the highest expression levels in HGC27 cells (Fig. 1F). These findings indicated that LINC00467 upregulation in GC was associated with the progression of GC.

Table I. Association between LINC00467 expression levels and clinicopathologic characteristics of patients with GC.

Patient characteristics	LINC00467 expression		P-value
	Low, n (%)	High, n (%)	
Age, years			
<60	12 (20.0)	11 (18.3)	0.791
≥60	18 (30.0)	19 (31.7)	
Sex			
Men	24 (40.0)	21 (35.0)	0.371
Women	6 (10.0)	9 (15.0)	
Differentiation			
Well and moderate	9 (15.0)	14 (23.3)	0.184
Poor and mixed	21 (35.0)	16 (26.7)	
Lauren type			
Intestinal	3 (5.0)	4 (6.7)	0.688
Diffused	27 (45.0)	26 (43.3)	
T stage			
T1-T3	24 (40.0)	27 (45.0)	0.278
T4	6 (10.0)	3 (5.0)	
N stage			
N0	3 (5.0)	11 (18.3)	0.015[a]
N1-N3	27 (45.0)	19 (31.7)	
M stage			
M0	25 (41.7)	29 (48.3)	0.085
M1	5 (8.3)	1 (1.7)	
TNM stage			
I and II	6 (10.0)	14 (23.3)	0.028[a]
III and IV	24 (40.0)	16 (26.7)	

P-values were calculated using the χ^2 test. [a]P<0.05. GC gastric cancer.

Knockdown of LINC00467 inhibits GC cell malignancy in vitro and in vivo. To explore the functional role of LINC00467 in GC cells, the LINC00467 expression was silenced using siRNA (Fig. 2A). The siRNA with the greatest knockdown efficiency (si-R1) was used in subsequent assays. Silencing of LINC00467 was found to suppress HGC27 cell proliferation in RTCA (Fig. 2B) and colony formation (Fig. 2C) assays. EdU assays demonstrated that the knockdown of LINC00467 also reduced EdU uptake compared with transfection with the control si-NC (Fig. 2D). LINC00467 silencing suppressed the proliferation of MKN45 cells (Fig. S2). In order to explore the mechanism underlying the modulation of GC tumor growth by LINC00467, the effects of si-LINC00467 transfection on invasive and migratory activity were examined with wound healing assays, which demonstrated that knockdown decreased the migration of HGC27 cells (Fig. 2E). Transwell assays further demonstrated that the knockdown of LINC00467 suppressed the migratory and invasive activity of HGC27 cells (Fig. 2F). The functional impact of LINC00467 knockdown on tumor growth was then assessed *in vivo* by transducing HGC27 cells with LINC00467-specific or control short hairpin (sh) RNAs and implanted them subcutaneously into the nude mice. Tumors derived from LINC00467-silenced cells grew more slowly and were smaller in size compared with sh-NC control tumors (Fig. 2G and H). The number of liver metastases were also significantly decreased in mice implanted with shLINC00467-expressing tumors compared with those implanted with control tumors (Fig. 2I and J; P=0.0376), which suggested that the loss of shLINC00467 was sufficient to interfere with the metastatic ability of HGC27 cells. Together, the findings suggested that knockdown of LINC00467 suppresses the growth of GC cells.

LINC00467 modulation influences glycolytic metabolism in GC cells. The findings from the analysis of GSE63089 demonstrated that LINC00467 serves a key role in metabolic pathways (Fig. S1E). The results demonstrated that silencing LINC00467 led to a significant decrease in glucose consumption, ATP production (Fig. 3A and B) and lactate production (Fig. 3C) in both MKN45 and HGC27 cell lines. Additionally, assessments of the ECAR and OCR further confirmed the impact of LINC00467 on aerobic glycolysis in GC cells (Fig. 3A). Specifically, LINC00467 knockdown resulted in a decrease in ECAR, which were associated with a decrease in glycolytic flux and an increase in OCR, and suggested enhanced mitochondrial respiration (Fig. 3D-G). In summary, these findings suggested that the downregulation of LINC00467 decreases aerobic glycolysis in GC cells.

LINC00467 binds to and sequesters miR-141-3p in GC cells. Predictive analyses suggested that LINC00467 is primarily localized in the cytoplasm of human cells (Figs. S3A and 3B). To evaluate the location, nuclear and cytoplasmic cell fractions were analyzed using qPCR, which confirmed the presence of LINC00467 in both the cytoplasm (>50%) and the nucleus (<50%) (Fig. 4A), and FISH analyses of human tissue samples, which yielded similar results (Fig. 4B). A prediction analysis on potential target genes of LINC00467 was conducted using bioinformatics tools including miTarget, TargetScan and StarBase, which indicated a putative binding site for miR-141-3p within LINC00467, consistent with the downregulation in GC cells. Subsequent investigations included the assessment of miR-141-3p expression in GC cells (Fig. 4C). Biotinylated miR-141-3p mimics and corresponding mutant plasmids were designed and transfected into MKN45 and HGC27 cells for a biotin pulldown assay. Notably, LINC00467 exhibited higher enrichment in the precipitate of WT biotin-coupled miR-141-3p compared with the corresponding mutant plasmids (Fig. 4D), which indicated a potential interaction through base pairing. Given the reported role of lncRNAs in sequestering miRNAs in an AGO2-dependent manner (28), the enrichment of LINC00467 following AGO2 immunoprecipitation in GC cells transfected with WT or mutated miR-141-3p mimics was evaluated. Enhanced enrichment of LINC00467 in WT miR-141-3p-transfected cells suggested the involvement of AGO2 in facilitating the interaction between LINC00467 and miR-141-3p (Fig. 4E and F). Subsequent FISH assays confirmed the co-localization of LINC00467 and miR-141-3p in the cytoplasm of MKN45 and HGC27 cells (Fig. 4G). Furthermore, bioinformatic analyses and luciferase reporter

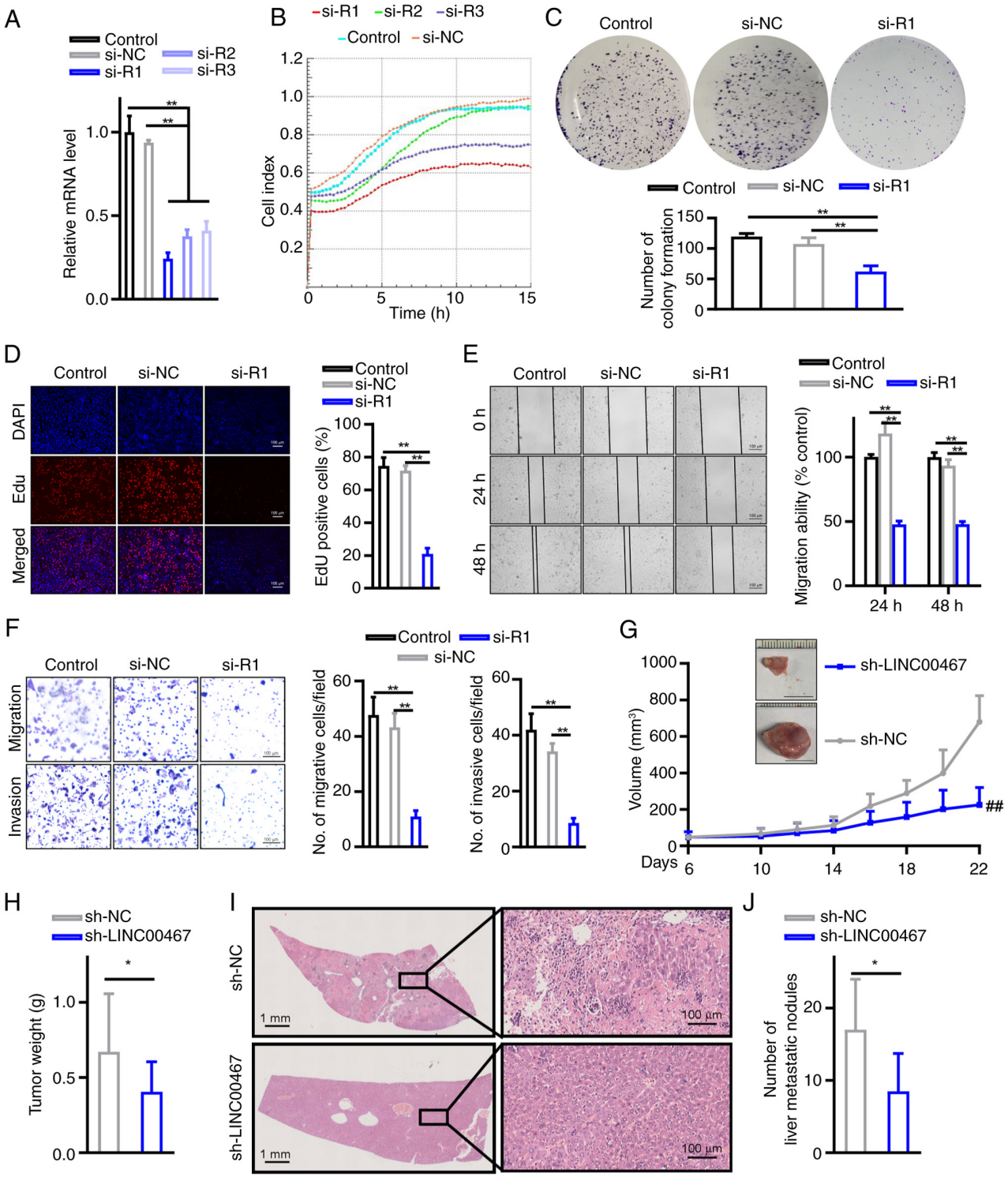

Figure 2. Knockdown of LINC00467 suppresses GC cell proliferation and invasion *in vitro* and *in vivo*. HGC27 cells exhibited (A) reduced LINC00467 expression following si-LINC00467 transfection and led to reduced proliferation demonstrated by (B) RTCA and (C) colony formation assays. (D) Si-LINC00467 transfection suppressed EdU uptake by HGC27 cells (scale bar, 100 μm). (E) Transfection of HGC27 cells with si-LINC00467 was associated with reduced migration in a wound healing assay and (F) reduced migration and invasion in Transwell assays compared with si-NC transfection. (G) Tumor volumes were assessed every other day in nude mice injected with HGC27 cells that had been transduced with sh-LINC00467 or sh-NC, demonstrating that LINC00467 knockdown was associated with reduced tumor growth. (H) Quantification of tumor weights (g). (I) Representative images of livers from mice in the two treatment groups (scale bar, 100 μm), with (J) corresponding quantification of the numbers of metastatic nodules. Data are presented as mean ± SD. **P<0.01 vs. si-NC; *P<0.05 vs. sh-NC; $^{\#\#}$P<0.01 vs. sh-NC. GC, gastric cancer; RTCA, real-time cell analysis; EdU, 5-Ethynyl-2'-deoxyuridine; NC, negative control; si-NC, small interfering RNA-NC; sh-NC, short hairpin RNA-NC.

assays corroborated the association between LINC00467 and miR-141-3p, which underscored the downregulation of miR-141-3p in GC tissues compared with normal tissues (Fig. 4H and I). Spearman's correlation analyses demonstrated a negative correlation between LINC00467 and miR-141-3p (r=-0.2951; P=0.0221; Fig. 4J).

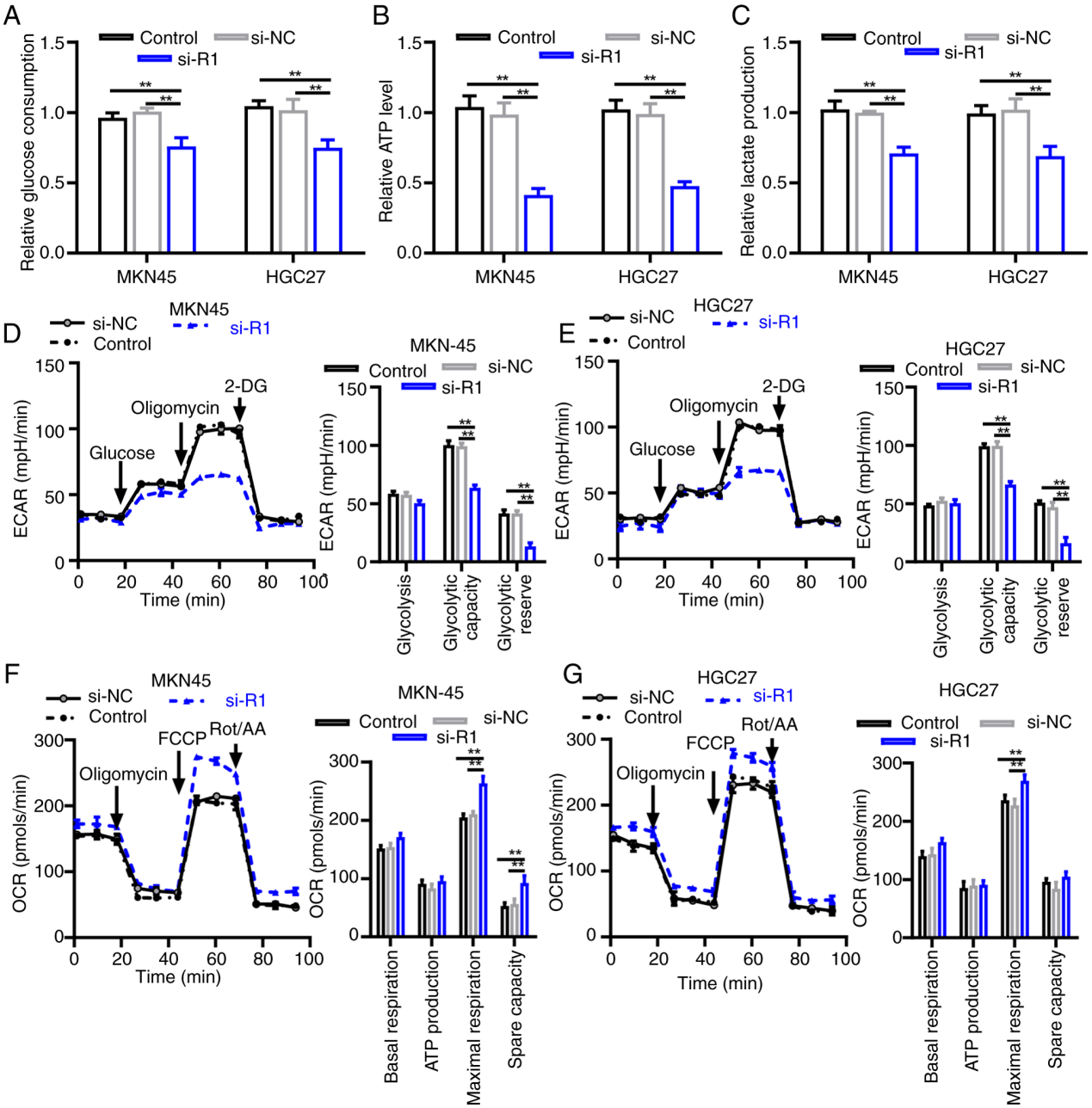

Figure 3. LINC00467 promotes glycolysis in GC cells. (A) Changes in relative glucose consumption, (B) ATP levels and (C) lactate production in MKN45 and HGC27 cells after LINC00467 knockdown. Changes in ECAR and OCR levels after LINC00467 knockdown in MKN45 and HGC27 cells. Effects of LINC00467 on glycolysis in (D) MKN45 and (E) HGC27 cells were assessed by ECAR following LINC00467 knockdown. ECAR assay and quantification of (D, right) MKN45 and (E, right) HGC27 cells; OCR assay and quantification of (F) MKN45 and (G) HGC27 cells transfected with LINC00467 knockdown. Quantifications of the OCR results of (F, right) MKN45 and (G, right) HGC27 cells, demonstrated basal respiration, ATP production, maximal respiration and spare capacity. **P<0.01. GC, gastric cancer; ECAR, extracellular acidification rate; OCR, oxygen consumption rate; si-NC, small interfering RNA-negative control; 2-DG, 2-deoxyglucose; FCCP, p-trifluoromethoxy carbonyl cyanide phenylhydrazone; Rot/AA, rotenone and antimycin A.

The possibility of mutual regulation between LINC00467 and miR-141-3p was then evaluated. The transfection of HGC27 and MKN45 cells with miR-141-3p inhibitors and mimics significantly decreased and increased expression levels, respectively (Fig. 5A and B; both P<0.0001). In order to investigate interactions between LINC00467 and miR-141-3p, luciferase reporter constructs containing WT or mutant (Mut LINC00467) versions of the putative miR-141-3p binding site in LINC00467 were prepared, which demonstrated that transfection with the miR-141-3p mimic was sufficient to suppress the activity of the WT but not Mut LINC00467 reporter vectors (Fig. 5C) in MKN45 cells. LINC00467 knockdown also significantly increased the expression of miR-141-3p (Fig. 5D; P<0.0001), whereas miR-141-3p silencing or overexpression led to increased or decreased LINC00467 expression, respectively (Fig. 5E and F). Thus, the results suggested that LINC00467 may function as a ceRNA that sequesters miR-141-3p in GC cells.

LINC00467 modulates GC cell malignancy by sequestering miR-141-3p. LINC00467 bonded to miR-141-3p, which suggested that LINC00467 may serve as a ceRNA for binding

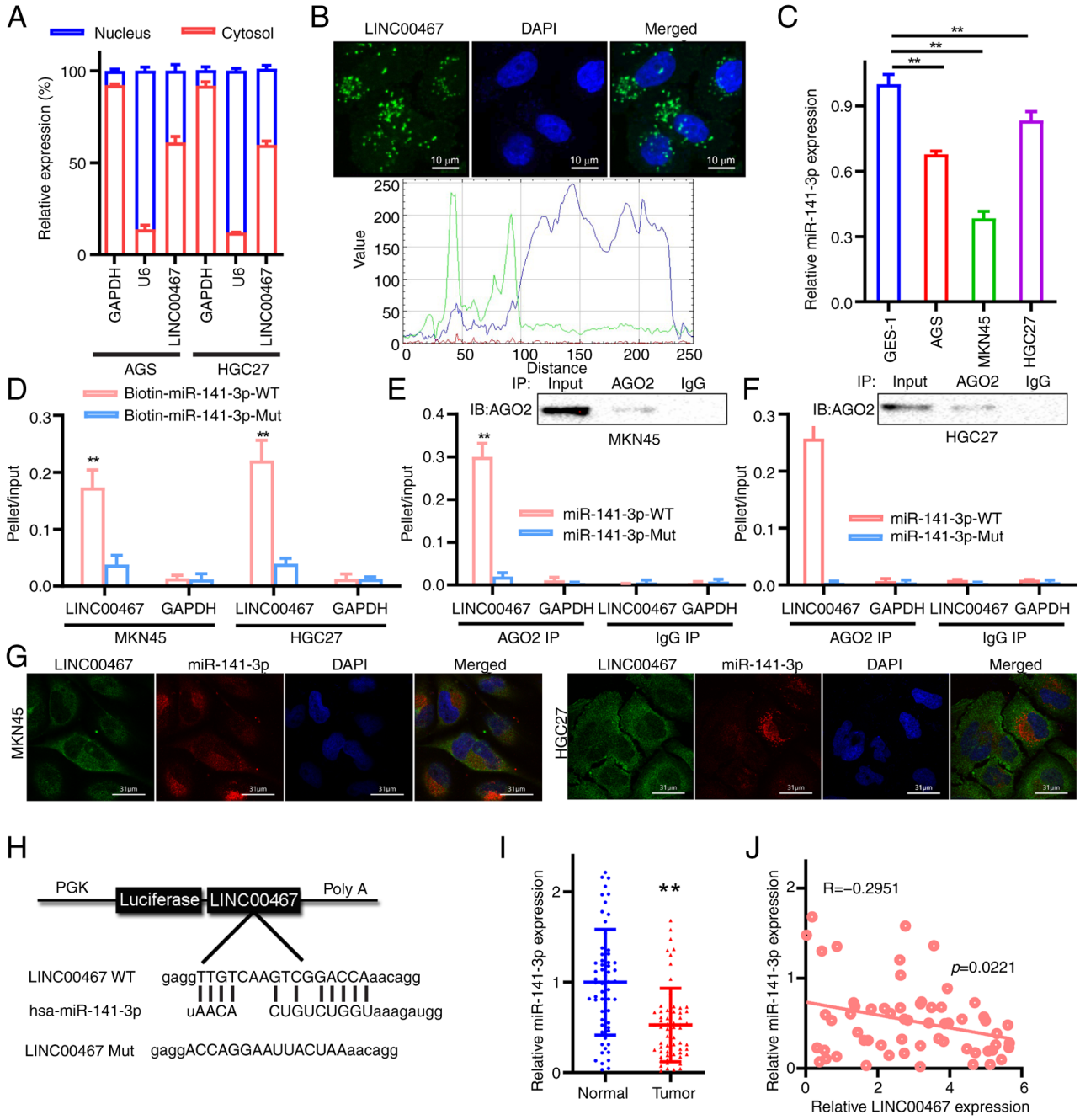

Figure 4. miR-141-3p is a LINC00467 target in GC cells. (A) Relative LINC00467 expression percentage in nuclear and cytoplasmic compartments was evaluated using U6 and GAPDH as respective nuclear and cytoplasmic normalization controls in AGS and HGC27 cell lines. (B) FISH was used to assess LINC00467 localization in GC cells and ImageJ was used to quantify confocal images (scale bar, 10 mm). (C) Relative miR-141-3p expression levels in control and GC cell lines (AGS, MKN45 and HGC27). (D) Expression levels of LINC00467 and GAPDH mRNA after streptavidin capture were measured in GC cells transfected with biotinylated miR-141-3p-WT or -Mut. (E) MKN45 and (F) HGC27 cells were transfected with miR-141-3p-WT or -Mut. (G) Representative FISH images demonstrated the co-localization of LINC00467 and miR-141-3p (scale bar, 31 μm). (H) Putative miR-141-3p-binding sites within the LINC00467 sequence, with corresponding schematics of the WT and Mut luciferase reporter vectors. (I) Relative miR-141-3p expression was assessed in 60 GC and normal para-cancerous tissue samples. **P<0.01. (J) The relationship between LINC00467 and miR-141-3p was assessed via Spearman correlation analyses in 60 GC samples. r=-0.2951; P<0.05. WT, wild-type; Mut, mutant; AGO2, argonaute 2; miR-141-3p, microRNA-141-3p; FISH, fluorescence *in situ* hybridization.

and sequestration of the miRNA. The RTCA and colony formation assay results indicated that transfection with the miR-141-3p inhibitor reversed the effects of LINC00467 knockdown on GC cell proliferation, demonstrated by RTCA assays (Fig. 6A) and colony assays (Fig. 6B). Transwell assays demonstrated that transfection with the miR-141-3p inhibitor reversed the LINC00467 knockdown-dependent reductions in migration and invasion by GC cells (Fig. 6C). Together, these results suggested that LINC00467 knockdown suppressed GC oncogenesis via a mechanism dependent upon miR-141-3p sequestration.

miR-141-3p as a direct regulator of DPYSL3 within the context of GC. miR-141-3p was identified as a direct regulator of DPYSL3 in GC, with computational analyses indicating a putative binding site within the 3'-UTR of DPYSL3 (Fig. 7A). Validation through luciferase reporter assays in MKN45 cells

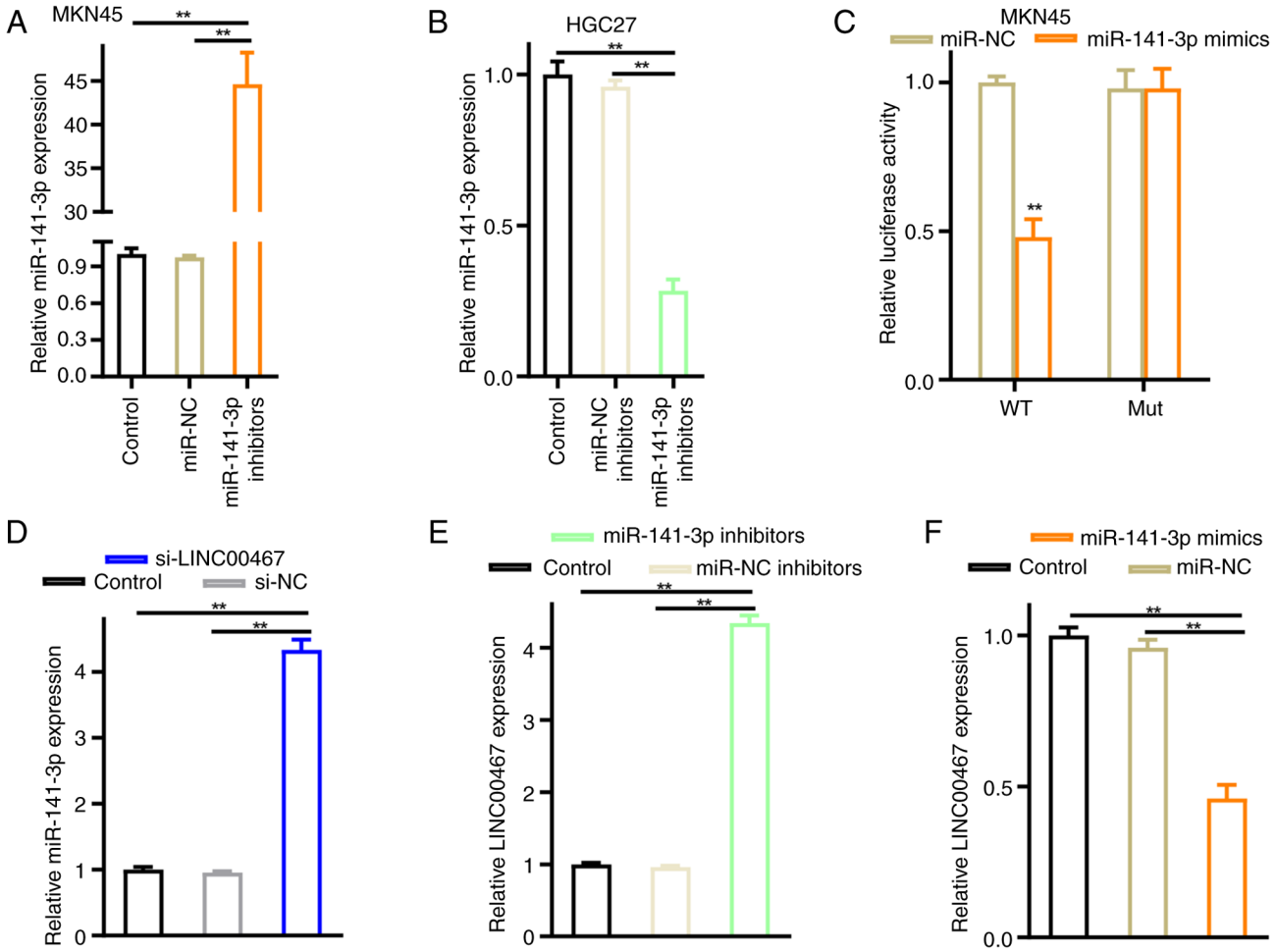

Figure 5. LINC00467 and miR-141-3p regulated one another. Relative miR-141-3p expression levels were assessed following transfection with an miR-141-3p mimic or control miR-NC in (A) MKN45 and (B) HGC27 cells. (C) MKN45 cells were co-transfected with WT or Mut LINC00467 vectors along with miR-141-3p mimics or miR-NC, after which luciferase activity was assessed. (D) Knockdown of LINC00467 significantly increased miR-141-3p expression in GC cells. (E) Transfection of HGC27 cells with the miR-141-3p inhibitor resulted in LINC00467 upregulation. (F) Transfection of MKN45 cells with miR-141-3p mimics resulted in LINC00467 downregulation. **P<0.01. miR-141-3p, microRNA-141-3p; miR-NC, microRNA negative control; WT, wild-type; Mut, mutant; GC, gastric cancer.

confirmed the binding interaction (Fig. 7B). Subsequent investigations demonstrated downregulation of DPYSL3 at both mRNA (Fig. 7C) and protein levels (Fig. 7D) in HGC27 cells post-transfection with si-LINC00467, while transfection with miR-141-3p mimics led to significantly decreased DPYSL3 expression levels (Fig. 7E and F). Notably, analysis of the AKT pathway involvement in GC cell metabolism demonstrated that DPYSL3 knockdown in MKN45 cells significantly attenuated GLUT1 expression without affecting HK2 and lactate dehydrogenase A/C expression (Fig. 7G; P<0.0001) (29,30). These findings suggest a mechanism wherein DPYSL3 facilitates glucose influx via increased GLUT1 expression, thereby potentially activating the AKT signaling pathway.

LINC00467/miR-141-3p/DPYSL3 axis in GC pathogenesis. Validation experiments were conducted to confirm the mechanism by which LINC00467 induced GC cell proliferation, migration and invasion via the LINC00467/miR-141-3p/DPYSL3 axis. Rescue experiments employing a miR-141-3p inhibitor and mimics were designed to investigate LINC00467's role in tumorigenesis. Analysis via qPCR and western blotting demonstrated that LINC00467 knockdown resulted in decreased mRNA and expression levels of DPYSL3 in MKN45 cells (Fig. 8A), while upregulation of LINC00467 significantly enhanced DPYSL3 expression levels in AGS cells (Fig. 8B). Additionally, the effects observed upon silencing or overexpressing LINC00467 were reversed by the miR-141-3p inhibitor or mimics, respectively (Fig. 8A and B). Further analyses sought to determine if the biological functions of LINC00467 in GC cells could be modulated by the miR-141-3p inhibitor or mimics. Results indicated that the miR-141-3p inhibitor counteracted the suppression of proliferation, migration and invasion caused by LINC00467 knockdown in MKN45 cells, while miR-141-3p mimics offset the promotion of these activities induced by upregulation of LINC00467 in AGS cells, as evidenced by colony formation and Transwell assays (Fig. 8C-E). Comprehensively, these findings underscore functionality of LINC00467 as a ceRNA for miR-141-3p, orchestrating DPYSL3 expression and in turn, contributing to the progression of GC.

Discussion

Although it has been found that lncRNAs can modulate the pathogenesis of GC, the functional importance of LINC00467

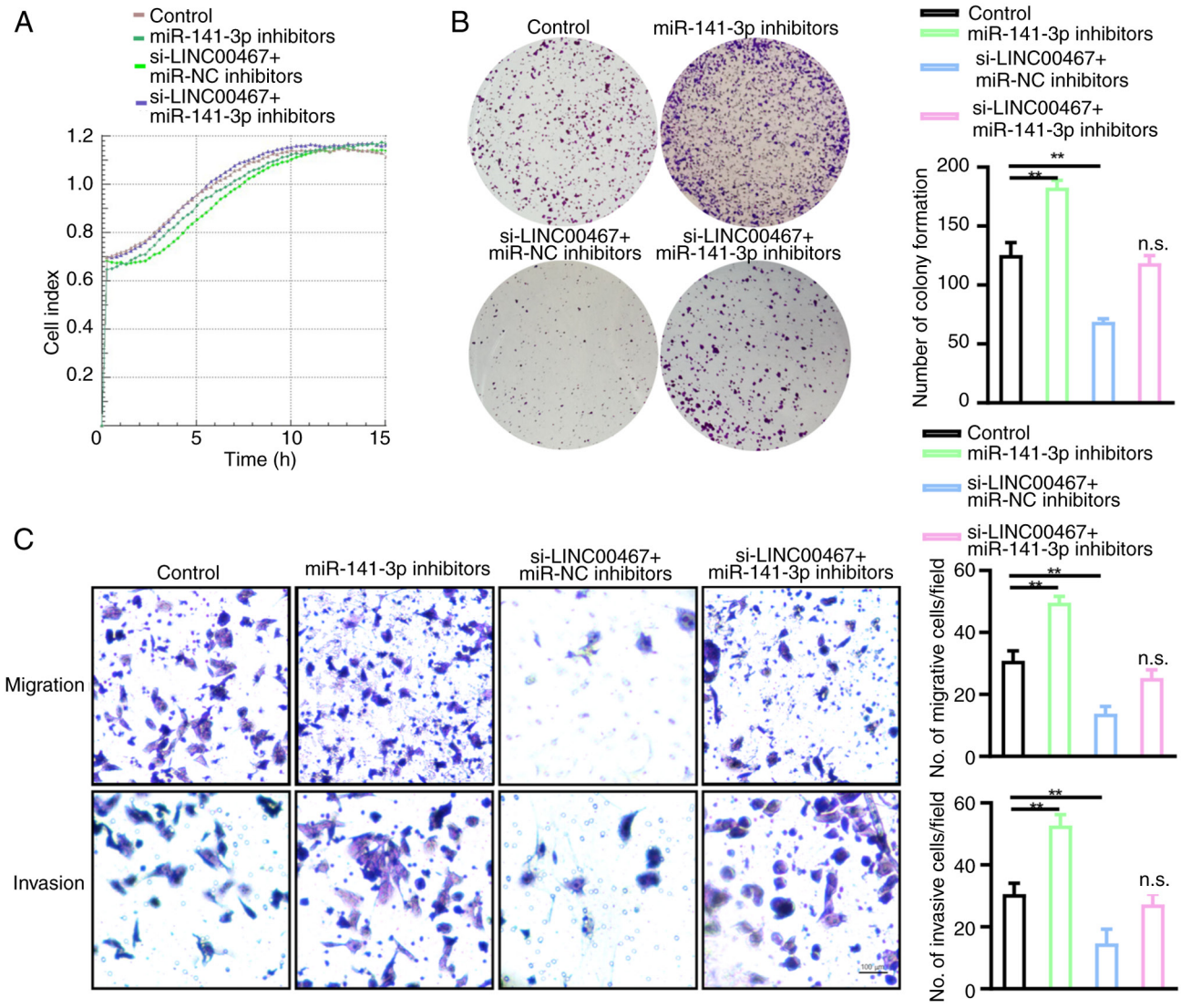

Figure 6. The impact of LINC00467 knockdown on GC cell malignancy was mediated by miR-141-3p. HGC27 cells were transfected with si-LINC00467 and miR-141-3p inhibitors or corresponding control constructs, after which (A) RTCA and (B) colony formation assays demonstrated that inhibition of miR-141-3p reversed the effects of LINC00467 knockdown on proliferation. (C) Transwell assays demonstrated that miR-141-3p inhibition reversed the effects of LINC00467 knockdown on GC cell migration and invasion. **P<0.01 vs. miR-NC. ns, not significant; miR-141-3p, microRNA-141-3p; RTCA, real-time cell analysis; miR-NC, microRNA negative control; GC, gastric cancer.

in this context remains to be clarified (31-33). LINC00467 is encoded on chromosome 1q32.3 in humans, and has been upregulated in non-small cell lung cancer, HCC and colorectal cancer, where it is suggested to be a risk factor associated with tumor progression (14,34,35). In the present study, the findings demonstrated that LINC00467 bound competitively to miR-141-3p, which resulted in the sequestration of the miRNA and upregulation of the miR-141-3p target gene, DPYSL3, and promoted GC development.

Significant LINC00467 upregulation was observed in both GC tumors and cell lines (AGS, P=0.0024; HGC27, P=0.0009; and MKN45, P<0.0001), and determined that the upregulation was associated with GC progression in patients. Consistent with this, earlier studies have reported LINC00467 to be of prognostic relevance in colorectal cancer (36) and HCC (15). The functional relevance of this lncRNA was then assessed in GC. In a previous study, Gao *et al* (37) demonstrated that LINC00467 promoted the proliferation, survival and migration of glioma cells through modulation of the miR-200a/E2F3 axis, while Liu *et al* (34) reported that LINC00467 could function as an oncogene in esophageal squamous cell carcinoma by sequestering miR-485-5p and thereby alter the expression levels of DPAGT1. Consistent with these findings, significantly reduced migration, growth and invasion were observed in GC cells following LINC00467 knockdown.

The ability of lncRNAs to control tumor cell malignancy is often linked to their regulation of specific miRNAs, which enable them to indirectly regulate downstream target genes such as ZEB1, c-Myc and MMP2 (38-40). A number of studies have demonstrated the ability of lncRNAs to modulate cellular biology by competitively binding to and sequestering miRNAs, thereby preventing them from repressing target gene expression (38-40). Through predictive bioinformatics analyses, LINC00467 was likely to serve as a ceRNA which was capable of negatively regulating miR-141-3p in GC cells; which was notable, as miR-141-3p

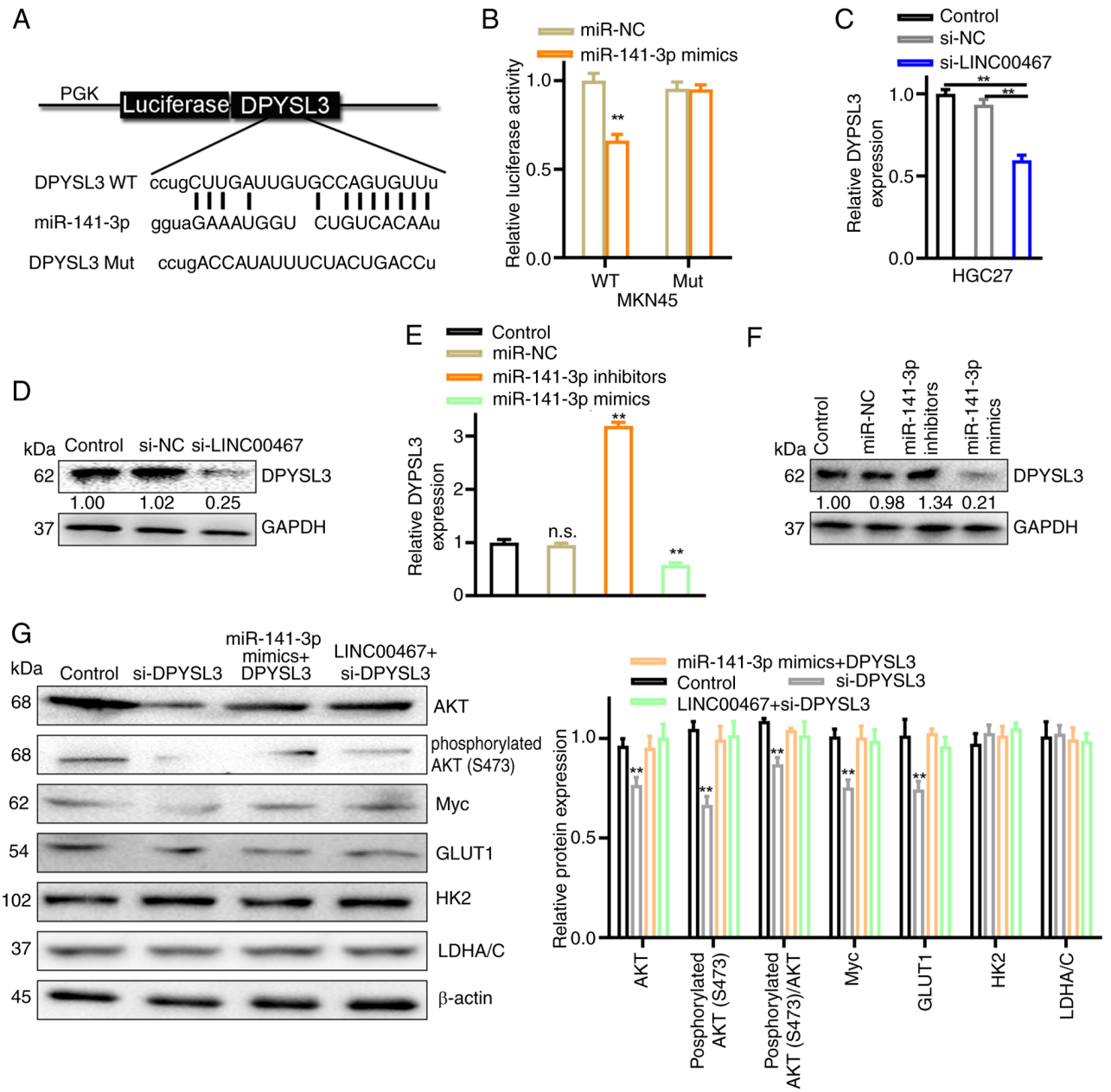

Figure 7. DPYSL3, a miR-141-3p target, was indirectly controlled by LINC00467. (A) WT and Mut DPYSL3 3'-UTR sequences. (B) Luciferase reporter assays were used to assess interactions between miR-141-3p interactions with the DPYSL3 3'-UTR, following transfection of MKN45 cells with the miR-141-3p mimics and luciferase reporter vectors containing the WT or Mut DPYSL3 3'-UTR. (C) Relative DPYSL3 mRNA expression levels in HGC27 cells was reduced following LINC00467 knockdown. LINC00467 knockdown in HGC27 cells reduced DPYSL3 protein expression levels (D). Effects of miR-141-3p overexpression and knockdown on DPYSL3 (E) mRNA and (F) protein expression levels, in HGC27 cells. (G) Relationship between DPYSL3 and AKT, Myc and GLUT1 associated with the AKT signaling pathway was explored by Western blotting analysis. **P<0.01, vs. miR-NC. PGK, phosphoglycerate kinase; GLUT1, glucose transporter 1; HK2, hexokinase 2; LDHA/C, lactate dehydrogenase A/C isoforms; WT, wild-type; Mut, mutant; NC, negative control; si-NC, small interfering RNA-NC; miR-141-3p, microRNA-141-3p; DPYSL3, dihydropyriminidase-like 3; miR-NC, microRNA-NC.

is a member of the miR-200 family and is directly relevant to the growth of tumors (41).

Increased expression levels of miR-141 in pancreatic cancer has been associated with improved patient outcomes (42). A range of miR-141 targets have been identified in pancreatic cancer, including MAP4K4, which is associated with the ability of this miRNA to control tumor cell malignancy and migration (42). Similarly, miR-141 can suppress TM4SF1 expression levels to inhibit migration and invasion in pancreatic cancer cells (43), and can also target WIPF1 to regulate metastasis in pancreatic cancer cells (44).

A subgroup analysis demonstrated that increased circulating miR-141 levels were associated with reduced patient survival, whereas increased tissue miR-141 levels were linked to improved patient prognosis, which suggest a context-specific role for miR-141 (45). In the present study, miR-141-3p downregulation in GC tissues and cells was observed and miR-141-3p expression levels were negatively correlated with that of LINC00467. From a functional perspective, inhibition of miR-141-3p reversed the effects of LINC00467 knockdown on GC cell malignancy and LINC00467 was observed to function as a ceRNA that can sequester miR-141-3p and regulate

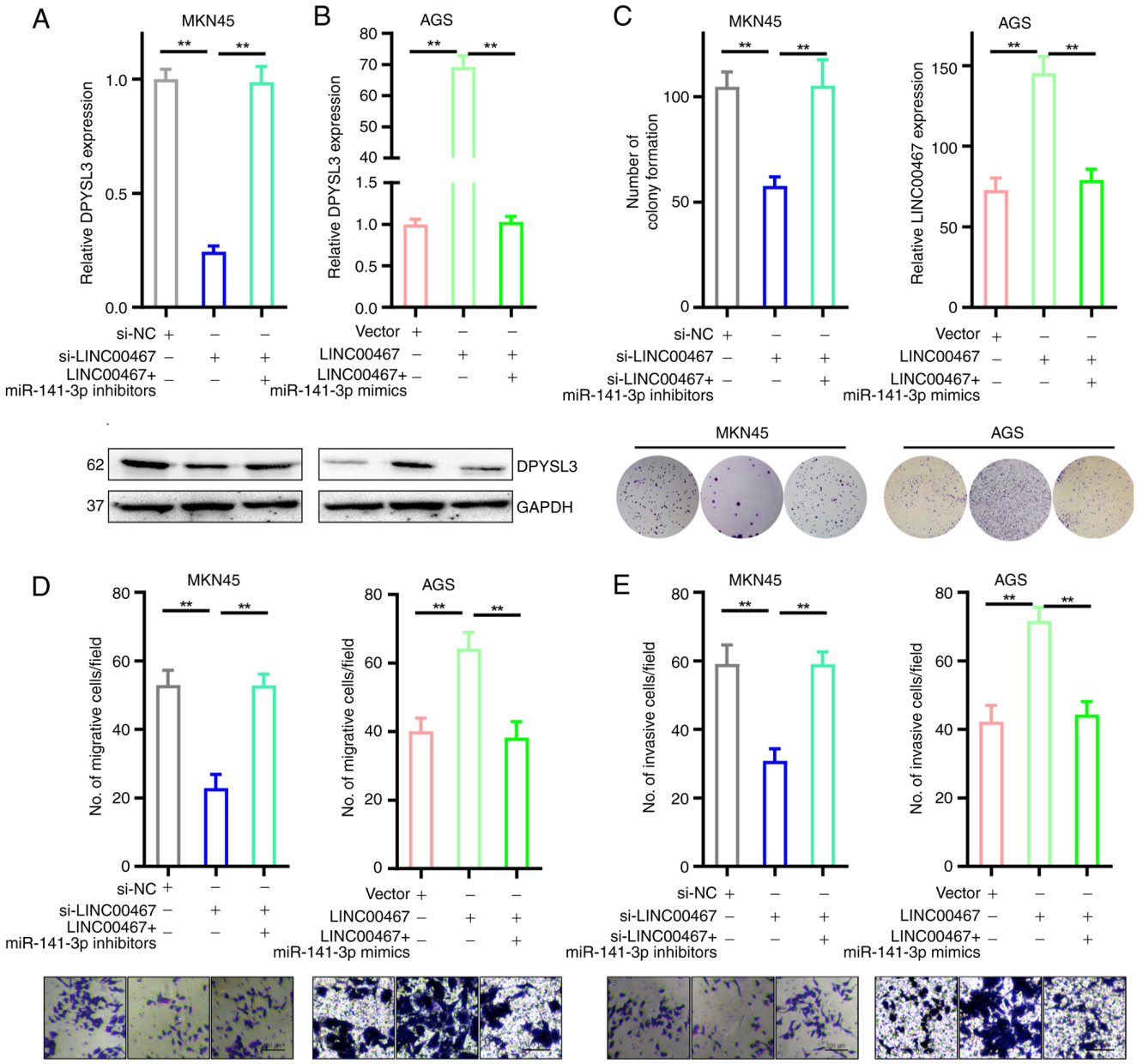

Figure 8. LINC00467 suppressed GC cell proliferation, migration and invasion through the LINC00467/miR-141-3p/DPYSL3 axis. Relative mRNA and protein expression levels of DPYSL3 in (A) MKN45 and (B) AGS cells transfected with miR-141-3p mimics and inhibitors, si-NC, si-LINC00467, or LINC00467, using qPCR and Western blotting, respectively. (C) Colony formation assays were used to assess proliferation in MKN45 and AGS cells transfected with miR-141-3p mimics and inhibitors, si-NC, si-LINC00467, or LINC00467. (D) Cell migration and (E) invasion was assessed using Transwell assays in MKN45 and AGS cells, respectively, following transfection with the miR-141-3p mimics and inhibitors, si-NC, si-LINC00467 and OV-LINC00467 (scale bar, 100 μm). Data were indicated as mean ± SD. **P<0.01. GC, gastric cancer; miR-141-3p, microRNA-141-3p; DPYSL3, dihydropyriminidase-like 3; si-NC, small interfering RNA-negative control.

its activity. The present study further confirmed the identity of DPYSL3 as a downstream miR-141-3p target in GC.

The cell adhesion molecule DPYSL3 has been purportedly linked to tumor metastasis, although differing results obtained in different tumor types suggest that it may function in a tumor-specific manner (46). The expression of DPYSL3 in prostate cancer was negatively associated with VEGF expression and lymph node metastasis in a mouse model using DPYSL3-overexpressing cells (47), and DPYSL3 was associated with enhanced adhesion, migration and metastasis of pancreatic cancer cells through the activation of a series of adhesion-related genes, such as FAK, TLN1 and c-Src (48). Other studies have suggested that DPYSL3 is also associated with GC cell malignancy (49,50) and while the present study did not specifically alter the levels of DPYSL3, others have found that the loss of DPYSL3 can result in GC cell cycle arrest (49). Findings from the present study demonstrated that miR-141-3p functioned as a post-transcriptional regulator of DPYSL3 expression such that LINC00467 knockdown indirectly downregulated the gene, which indicates that LINC00467 may control GC cell functionality via the miR-141-3p/DPYSL3 axis.

LINC00467 expression was found to be upregulated by increased levels of glycolysis in the present study. Moreover, there is increasing evidence which suggests that lactate,

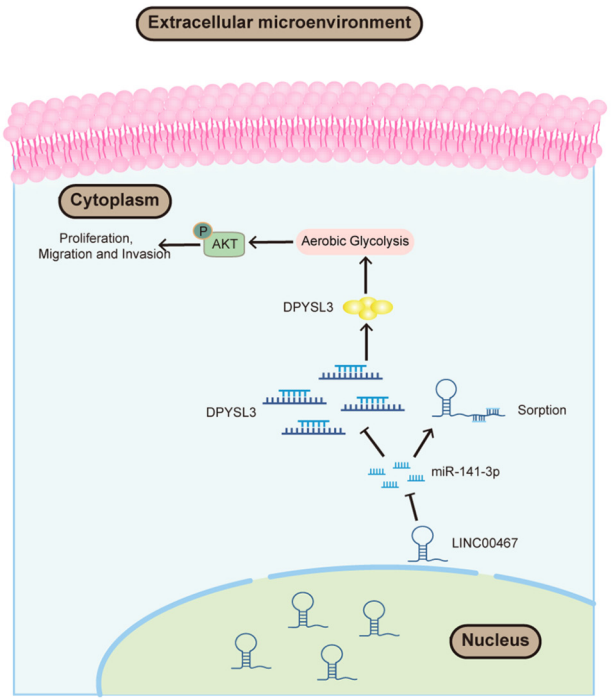

Figure 9. Molecular mechanism associated with the effects of LINC00467 on GC progression via regulation of miR-141-3p and DPYSL3. LINC00467 promoted glycolysis in GC cells and enhanced tumor cell proliferation, migration and invasion. LINC00467 specifically competed with miR-141-3p and downregulation of LINC00467 could upregulate the expression levels of miR-141-3p and downregulate DPYSL3 expression levels, and thus regulate aerobic glycolysis, inhibit proliferation, migration and invasion in GC cells. GC, gastric cancer; miR-141-3p, microRNA-141-3p; DPYSL3, dihydropyrimidinase-like 3.

a metabolite of glycolysis, serves a notable role in reprogramming the microenvironment associated with tumor metastasis (51). Additionally, LINC00467 upregulation in GC cell lines (AGS, HGC27 and MKN45) in response to lactate was observed. Mechanistically, results from the present study demonstrated that lactate acted as an inducer of LINC00467 and formed a feedback loop through activation of the AKT signaling pathway. Although previous studies have reported that lactate activates the AKT signaling pathway, the present study provides further evidence that this pathway is involved in LINC00467 regulation. Additionally, lactate has been demonstrated to promote the expression of pyrroline-5-carboxylate reductase 1 (PYCR1) via the AKT pathway (52,53). Advanced tumors are capable of regulating their own microenvironment and have the potential to disrupt global homeostasis, as recently discussed in a study which highlighted how cancer can hijack the body's homeostasis through the neuroendocrine system (54). This concept emphasizes the complexity of cancer progression, where tumors can exert systemic effects beyond their local environment (55). In the present study, the upregulation of LINC00467 in GC and its role in promoting glycolysis and tumor progression may be part of a broader mechanism through which GC cells alter both local and systemic homeostasis. This highlights the importance of understanding the multifaceted interactions between cancer cells and the physiological systems, which could have implications for therapeutic strategies targeting not only tumor growth but also systemic effects of cancer. Results from the present study demonstrated a novel aspect of the role of AKT in the regulation of lncRNA expression, shedding light on a previously unknown mechanism connecting the AKT pathway and glycolysis. However, it is not known whether AKT is activated directly by lactate accumulation during glycolysis. Further research is warranted to determine if other glycolytic metabolites are also implicated in this positive feedback loop.

The upregulation of aerobic glycolysis has been demonstrated to promote cancer progression and cellular proliferation by facilitating the generation of diverse metabolic intermediates key for numerous biological signaling pathways and acclimatizing to the tumor microenvironment (45). Consequently, targeting the reduction of aerobic glycolysis has emerged as a promising therapeutic approach in cancer management (56). Nonetheless, the intricate mechanisms through which lncRNA modulates aerobic glycolysis in GC cells remain inadequately explored (57). Within the scope of the present study, the findings demonstrated LINC00467 as a newly identified stimulator of aerobic glycolysis in GC, which exerted influence through the sequestration of miR-141-3p and subsequent elevation of DPYSL3 expression.

There were three primary limitations in the present study. First, all clinical analyses were retrospective in nature and further prospective research is necessary to confirm the clinical importance of LINC00467 in this oncogenic context. Second, although the LINC00467/miR-141-3p/DPYSL3 axis was linked to GC progression, the specific pathways whereby LINC00467 modulates GC tumor progression remain to be elucidated. Third, the main focus of the present study was the impact of LINC00467 knockdown on GC progression; future studies should evaluate the oncogenic impact of overexpression of LINC00467 in GC.

In conclusion, the expression of LINC00467 was upregulated in GC tumors and cell lines (AGS, HGC27 and MKN45) and that LINC00467 upregulation was associated with poor outcomes for patients with GC. LINC00467 promoted glycolysis in GC cells, which led to enhanced proliferative, migratory and invasive activity. Knockdown of LINC00467 suppressed the malignant activity of GC cells by sequestration of miR-141-3p and thereby upregulated DPYSL3 (Fig. 9), which suggested that the miR-141-3p/DPYSL3 signaling axis regulates GC development. These findings not only reveal LINC00467 as a potential prognostic biomarker for GC but also identify the LINC00467/miR-141-3p/DPYSL3 axis as a promising therapeutic target for disrupting glycolytic metabolism and tumor progression in GC, offering new strategies for clinical intervention.

Acknowledgements

Not applicable.

Funding

The present study was supported by the Program for Key research and development plan of Shandong province (grant no. 2017GSF18179), the Natural Science Foundations of Shandong Province (grant nos. ZR2021MH052 and ZR2021MH022), the Science and Technology Benefit for

the People Demonstration Special Project of Qingdao (grant nos. 23-2-8-smjk-3-nsh and 24-1-8-smjk-11-nsh), the Qingdao Shinan District Science and Technology Plan (grant no. 2022-4-010-YY), and and the 'Clinical Medicine + X' of Qingdao University (grant no. CMX201729).

Availability of data and materials

The data generated in the present study may be requested from the corresponding author.

Authors' contributions

HJ, SL and YF conceptualized the study. XM and WH were responsible for collecting the patient's information. XM, WH, GH, BT, SL and DC conducted the formal analysis for the study. CL and YS performed the experiments. HC, DC and CL devised the methodology for the study. XM, WH and GH supervised the experiments. HJ wrote the original draft of the manuscript. HJ, YF, XM, WH and SL wrote, reviewed and edited the manuscript. HJ and SL confirm the authenticity of all the raw data. All authors read and approved the final manuscript.

Ethics approval and consent to participate

The studies involving human participants were reviewed and approved by The Ethics Committee at the Affiliated Hospital of Qingdao University (approval no. AHQDGC2019022; Qingdao, China). The patients provided their written informed consent to participate in the present study. Written informed consent was obtained and signed from all participants. The Ethics Committee of the Affiliated Hospital of Qingdao University approved the present animal studies (approval no. AHQU-MAL20190810; Qingdao, China).

Patient consent for publication

Not applicable.

Competing interests

The authors declare that the they have no competing interests.

References

1. Filho AM, Laversanne M, Ferlay J, Colombet M, Piñeros M, Znaor A, Parkin DM, Soerjomataram I and Bray F: The GLOBOCAN 2022 cancer estimates: Data sources, methods, and a snapshot of the cancer burden worldwide. Int J Cancer 156: 1336-1346, 2025.
2. Dong D, Yu X, Xu J, Yu N, Liu Z and Sun Y: Cellular and molecular mechanisms of gastrointestinal cancer liver metastases and drug resistance. Drug Resist Updat 77: 101125, 2024.
3. de Back TR, van Hooff SR, Sommeijer DW and Vermeulen L: Transcriptomic subtyping of gastrointestinal malignancies. Trends Cancer 10: 842-856, 2024.
4. Zhang T, Chen Y and Xiang Z: Machine learning-based integration develops a disulfidptosis-related lncRNA signature for improving outcomes in gastric cancer. Artif Cells Nanomed Biotechnol 53: 1-13, 2025.
5. Vaghari-Tabari M, Qujeq D and Hashemzadeh MS: Long noncoding RNAs as potential targets for overcoming chemoresistance in upper gastrointestinal cancers. Biomed Pharmacother 179: 117368, 2024.
6. Shuai Y, Ma Z, Liu W, Yu T, Yan C, Jiang H, Tian S, Xu T and Shu Y: TEAD4 modulated LncRNA MNX1-AS1 contributes to gastric cancer progression partly through suppressing BTG2 and activating BCL2. Mol Cancer 19: 6, 2020.
7. Wu Q, Ma J, Wei J, Meng W, Wang Y and Shi M: lncRNA SNHG11 promotes gastric cancer progression by activating the Wnt/β-catenin pathway and oncogenic autophagy. Mol Ther 29: 1258-1278, 2020.
8. Zhou R, Sun H, Zheng S, Zhang J, Zeng D, Wu J, Huang Z, Rong X, Bin J, Liao Y, *et al*: A stroma-related lncRNA panel for predicting recurrence and adjuvant chemotherapy benefit in patients with early-stage colon cancer. J Cell Mol Med 24: 3229-3241, 2020.
9. Wang P, Guo Q, Hao Y, Liu Q, Gao Y, Zhi H, Li X, Shang S, Guo S, Zhang Y, *et al*: LnCeCell: A comprehensive database of predicted lncRNA-associated ceRNA networks at single-cell resolution. Nucleic Acids Res 49: D125-D133, 2021.
10. Tian Y, Ma R, Sun Y, Liu H, Zhang H, Sun Y, Liu L, Li Y, Song L and Gao P: SP1-activated long noncoding RNA lncRNA GCMA functions as a competing endogenous RNA to promote tumor metastasis by sponging miR-124 and miR-34a in gastric cancer. Oncogene 39: 4854-4868, 2020.
11. Ye J, Li J and Zhao P: Roles of ncRNAs as ceRNAs in gastric cancer. Genes (Basel) 12: 1036, 2021.
12. Liu HT, Ma RR, Lv BB, Zhang H, Shi DB, Guo XY, Zhang GH and Gao P: LncRNA-HNF1A-AS1 functions as a competing endogenous RNA to activate PI3K/AKT signalling pathway by sponging miR-30b-3p in gastric cancer. Br J Cancer 122: 1825-1836, 2020.
13. Zhang Y, Li J, Jia S, Wang Y, Kang Y and Zhang W: Down-regulation of lncRNA-ATB inhibits epithelial-mesenchymal transition of breast cancer cells by increasing miR-141-3p expression. Biochem Cell Biol 97: 193-200, 2019.
14. Zhu Y, Li J, Bo H, He D, Xiao M, Xiang L, Gong L, Hu Y, Zhang Y, Cheng Y, *et al*: LINC00467 is up-regulated by TDG-mediated acetylation in non-small cell lung cancer and promotes tumor progression. Oncogene 39: 6071-6084, 2020.
15. Li W, He Y, Chen W, Man W, Fu Q, Tan H, Guo H, Zhou J and Yang P: Knockdown of LINC00467 contributed to Axitinib sensitivity in hepatocellular carcinoma through miR-509-3p/PDGFRA axis. Gene Ther 28: 634-645, 2020.
16. Li Z, Liu J, Chen H, Zhang Y, Shi H, Huang L, Tao J, Shen R and Wang T: Ferritin light chain (FTL) competes with long noncoding RNA Linc00467 for miR-133b binding site to regulate chemoresistance and metastasis of colorectal cancer. Carcinogenesis 41: 467-477, 2020.
17. Wiel C, Le Gal K, Ibrahim MX, Jahangir CA, Kashif M, Yao H, Ziegler DV, Xu X, Ghosh T, Mondal T, *et al*: BACH1 stabilization by antioxidants stimulates lung cancer metastasis. Cell 178: 330-345, 2019.
18. Stine ZE, Schug ZT, Salvino JM and Dang CV: Targeting cancer metabolism in the era of precision oncology. Nat Rev Drug Discov 21: 141-162, 2022.
19. Wang Q, Yu PF, Liu CX, He XL and Wang G: Mitochondrial fragmentation in liver cancer: Emerging player and promising therapeutic opportunities. Cancer Lett 549: 215912, 2022.
20. Wang N, Tan HY, Lu YJ, Chan YT, Wang D, Guo W, Xu Y, Zhang C, Chen F, Tang G and Feng Y: PIWIL1 governs the crosstalk of cancer cell metabolism and immunosuppressive microenvironment in hepatocellular carcinoma. Signal Transduct Tar 6: 86, 2021.
21. Amin MB, Greene FL, Edge SB, Compton CC, Gershenwald JE, Brookland RK, Meyer L, Gress DM, Byrd DR and Winchester DP: The eighth edition AJCC cancer staging manual: Continuing to build a bridge from a population-based to a more 'personalized' approach to cancer staging. CA Cancer J Clin 67: 93-99, 2017.
22. Zhang X, Ni Z, Duan Z, Xin Z, Wang H, Tan J, Wang G and Li F: Overexpression of E2F mRNAs associated with gastric cancer progression identified by the transcription factor and miRNA co-regulatory network analysis. PLoS One 10: e0116979, 2015.
23. Ye L, Pu C, Tang J, Wang Y, Wang C, Qiu Z, Xiang T, Zhang Y and Peng W: Transmembrane-4 L-six family member-1 (TM4SF1) promotes non-small cell lung cancer proliferation, invasion and chemo-resistance through regulating the DDR1/Akt/ERK-mTOR axis. Respir Res 20: 106, 2019.
24. Liu S, Qiu J, He G, Liang Y, Wang L, Liu C and Pan H: LncRNA MALAT1 acts as a miR-125a-3p sponge to regulate FOXM1 expression and promote hepatocellular carcinoma progression. J Cancer 10: 6649-6659, 2019.
25. Livak KJ and Schmittgen TD: Analysis of relative gene expression data using real-time quantitative PCR and the 2(-Delta Delta C(T)) method. Methods 25: 402-408, 2001.

26. Moniri MR, Young A, Reinheimer K, Rayat J, Dai LJ and Warnock GL: Dynamic assessment of cell viability, proliferation and migration using real time cell analyzer system (RTCA). Cytotechnology 67: 379-386, 2015.
27. Laferriere CA, Leung VS and Pang DS: Evaluating intrahepatic and intraperitoneal sodium pentobarbital or ethanol for mouse euthanasia. J Am Assoc Lab Anim Sci 59: 264-268, 2020.
28. Zhao X, Su L, He XY, Zhao BX and Miao JY: Long noncoding RNA CA7-4 promotes autophagy and apoptosis via sponging MIR877-3P and MIR5680 in high glucose-induced vascular endothelial cells. Autophagy 16: 70-85, 2020.
29. Massari F, Ciccarese C, Santoni M, Iacovelli R, Mazzucchelli R, Piva F, Scarpelli M, Berardi R, Tortora G, Lopez-Beltran A, *et al*: Metabolic phenotype of bladder cancer. Cancer Treat Rev 45: 46-57, 2016.
30. Burns JE, Hurst CD, Knowles MA, Phillips RM and Allison SJ: The Warburg effect as a therapeutic target for bladder cancers and intratumoral heterogeneity in associated molecular targets. Cancer Sci 112: 3822-3834, 2021.
31. Hu Y, Zhang Y, Ding M and Xu R: LncRNA TMPO-AS1/miR-126-5p/BRCC3 axis accelerates gastric cancer progression and angiogenesis via activating PI3K/Akt/mTOR pathway. J Gastroenterol Hepatol 36: 1877-1888, 2020.
32. Ma P, Pan Y, Yang F, Fang Y, Liu W, Zhao C, Yu T, Xie M, Jing X, Wu X, *et al*: KLF5-modulated lncRNA NEAT1 contributes to tumorigenesis by acting as a scaffold for BRG1 to silence GADD45A in gastric cancer. Mol Ther Nucleic Acids 22: 382-395, 2020.
33. Ma ZH, Shuai Y, Gao XY, Yan Y, Wang KM, Wen XZ and Ji JF: BTEB2-activated lncRNA TSPEAR-AS2 drives GC progression through suppressing GJA1 expression and upregulating CLDN4 expression. Mol Ther Nucleic Acids 22: 1129-1141, 2020.
34. Liu Z, Yang S, Chen X, Dong S, Zhou S and Xu S: LncRNA LINC00467 acted as an oncogene in esophageal squamous cell carcinoma by accelerating cell proliferation and preventing cell apoptosis via the miR-485-5p/DPAGT1 axis. J Gastroenterol Hepatol 36: 721-730, 2020.
35. Zhang Y, Jiang X, Wu Z, Hu D, Jia J, Guo J, Tang T, Yao J, Liu H and Tang H: Long noncoding RNA LINC00467 promotes glioma progression through inhibiting P53 expression via binding to DNMT1. J Cancer 11: 2935-2944, 2020.
36. He X, Li S, Yu B, Kuang G, Wu Y, Zhang M, He Y, Ou C and Cao P: Up-regulation of LINC00467 promotes the tumourigenesis in colorectal cancer. J Cancer 10: 6405-6413, 2019.
37. Gao S, Duan H, An D, Yi X, Li J and Liao C: Knockdown of long non-coding RNA LINC00467 inhibits glioma cell progression via modulation of E2F3 targeted by miR-200a. Cell Cycle 19: 2040-2053, 2020.
38. Evans JR, Feng FY and Chinnaiyan AM: The bright side of dark matter: lncRNAs in cancer. J Clin Invest 126: 2775-2782, 2016.
39. Wei L, Sun J, Zhang N, Zheng Y, Wang X, Lv L, Liu J, Xu Y, Shen Y and Yang M: Noncoding RNAs in gastric cancer: Implications for drug resistance. Mol Cancer 19: 62, 2020.
40. Xie S, Chang Y, Jin H, Yang F, Xu Y, Yan X, Lin A, Shu Q and Zhou T: Non-coding RNAs in gastric cancer. Cancer Lett 493: 55-70, 2020.
41. Li M, Huang H, Cheng F, Hu X and Liu J: miR-141-3p promotes proliferation and metastasis of nasopharyngeal carcinoma by targeting NME1. Adv Med Sci 65: 252-258, 2020.
42. Zhao G, Wang B, Liu Y, Zhang JG, Deng SC, Qin Q, Tian K, Li X, Zhu S, Niu Y, *et al*: miRNA-141, downregulated in pancreatic cancer, inhibits cell proliferation and invasion by directly targeting MAP4K4. Mol Cancer Ther 12: 2569-2580, 2013.
43. Xu L, Li Q, Xu D, Wang Q, An Y, Du Q, Zhang J, Zhu Y and Miao Y: hsa-miR-141 downregulates TM4SF1 to inhibit pancreatic cancer cell invasion and migration. Int J Oncol 44: 459-466, 2014.
44. Pan Y, Lu F, Xiong P, Pan M, Zhang Z, Lin X, Pan M and Huang H: WIPF1 antagonizes the tumor suppressive effect of miR-141/200c and is associated with poor survival in patients with PDAC. J Exp Clin Cancer Res 37: 167, 2018.
45. Luo QQ, Tian Y, Qu GJ, Kun H and Luo SS: Functional mechanism and clinical implications of miR-141 in human cancers. Cell Signal 95: 110354, 2022.
46. Matsunuma R, Chan DW, Kim BJ, Singh P, Han A, Saltzman AB, Cheng C, Lei JT, Wang J, Roberto da Silva L, *et al*: DPYSL3 modulates mitosis, migration, and epithelial-to-mesenchymal transition in claudin-low breast cancer. Proc Natl Acad Sci USA 115: E11978-E11987, 2018.
47. Gao X, Pang J, Li LY, Liu WP, Di JM, Sun QP, Fang YQ, Liu XP, Pu XY, He D, *et al*: Expression profiling identifies new function of collapsin response mediator protein 4 as a metastasis-suppressor in prostate cancer. Oncogene 29: 4555-4566, 2010.
48. Kawahara T, Hotta N, Ozawa Y, Kato S, Kano K, Yokoyama Y, Nagino M, Takahashi T and Yanagisawa K: Quantitative proteomic profiling identifies DPYSL3 as pancreatic ductal adenocarcinoma-associated molecule that regulates cell adhesion and migration by stabilization of focal adhesion complex. PLoS One 8: e79654, 2013.
49. Kanda M, Nomoto S, Oya H, Shimizu D, Takami H, Hibino S, Hashimoto R, Kobayashi D, Tanaka C, Yamada S, *et al*: Dihydropyrimidinase-like 3 facilitates malignant behavior of gastric cancer. J Exp Clin Cancer Res 33: 66, 2014.
50. Zhong H and Luo X: Serum Dihydropyrimidinase-Like 3 concentration in patients with gastric cancer and its diagnostic value. Iran J Public Health 50: 1789-1795, 2021.
51. Zhao L, Liu YY, Zhang SM, Wei L, Cheng H, Wang J and Wang J: Impacts and mechanisms of metabolic reprogramming of tumor microenvironment for immunotherapy in gastric cancer. Cell Death Dis 13: 378, 2022.
52. Zhang CS, Cheng W, Yang TJ, Fang HL and Zhang RQ: Lactate secreted by esophageal cancer cells induces M2 macrophage polarization via the AKT/ERK pathway. Thorac Cancer 14: 2139-2148, 2023.
53. Li Z, Jiang Y, Liu J, Fu H, Yang Q, Song W and Li Y: Exosomes from PYCR1 knockdown bone marrow mesenchymal stem inhibits aerobic glycolysis and the growth of bladder cancer cells via regulation of the EGFR/PI3K/AKT pathway. Int J Oncol 63: 84, 2023.
54. Slominski RM, Raman C, Chen JY and Slominski AT: How cancer hijacks the body's homeostasis through the neuroendocrine system. Trends Neurosci 46: 263-275, 2023.
55. Swanton C, Bernard E, Abbosh C, André F, Auwerx J, Balmain A, Bar-Sagi D, Bernards R, Bullman S, DeGregori J, *et al*: Embracing cancer complexity: Hallmarks of systemic disease. Cell 187: 1589-1616, 2024.
56. Huang S, Shi J, Shen J and Fan X: Metabolic reprogramming of neutrophils in the tumor microenvironment: Emerging therapeutic targets. Cancer Lett 612: 217466, 2025.
57. Hou XR, Zhang ZD, Cao XL and Wang XP: Long noncoding RNAs, glucose metabolism and cancer (Review). Oncol Lett 26: 340, 2023.